

cosmological consequences and statefinder diagnosis of non-interacting generalized Chaplygin gas in $f(R, T)$ gravity

Hamid Shabani^{1, *}

¹*Physics Department, Faculty of Sciences, University of Sistan and Baluchestan, Zahedan, Iran*

(Dated: March 7, 2019)

In this paper, we investigate the cosmological consequences of a scenario for the recently reported accelerated expansion of the Universe, in which the generalized Chaplygin gas (GCG) and the baryonic matter are responsible for this observed phenomenon. Here, we have worked in an isotropic and homogeneous FLRW space time in $f(R, T)$ theory of gravity. In $f(R, T)$ gravity, the conservation of the energy-momentum tensor, leads to a constraint equation which enforces us to use some specific forms for the function $f(R, T)$. We consider three classes of models which include three different forms of $f(R, T)$ function; Class *I*, are those models which employ the standard Chaplygin gas (SCG), in class *II*, we use GCG in the high pressure regime and finally, models *III* make use of GCG in the high density regimes. The effective equation of state (EoS), the deceleration parameter for these models are calculated and showed that the related present values are more observationally acceptable in $f(R, T)$ gravity, compared to the corresponding ones in the General Relativity (GR). And, among them class *III* have a better situation; the predictions of these models are more consistent with the observational values. We also consider these models via the statefinder diagnosis tools. The statefinder parameters s and r are obtained for these three classes of models and the various trajectories are plotted for the different values of the model parameters. The involved parameters are, K and α which correspond to CG, \mathbf{m} , $\mathbf{n}^{(I)}$, $\mathbf{n}^{(II)}$ and $\mathbf{n}^{(III)}$ which come from the $f(R, T)$ function terms in the either classes. The discrimination between different dark energy models are considered by varying the mentioned parameters in the three types of models. Since, the positive values for \mathbf{m} and \mathbf{n} 's lead to some divergencies, we work on the positive values. It is discussed that the consistent values for the effective EoS for all allowed values of K , can only be obtained in Class II models. We show that the distance of the models to the Λ CDM model, varies for different choice of the model parameters. However, the distance is independent on the values of α for model *III*.

PACS numbers: 98.80.-k; 04.50.Kd; 95.36.+x; 98.80.Jk

Keywords: Cosmology; $f(R, T)$ Gravity; Dark Energy; Chaplygin gas; statefinder diagnosis.

I. INTRODUCTION

Currently, observational experiments show that the Universe has undergone an accelerated expansion [1–8]. The most accepted agreement is that there is two components which play a serious and important role in the formation and the evolution of the Universe; the “dark matter” (DM), that is responsible for the structure formation and the clustering of the galaxies [9–13] and the “dark energy” (DE) making a negative pressure gives rise to accelerated expansion of the Universe [14–17]. The former has the contribution of about 26% of the total matter density, the later forms about 69% of it and the rest is related to the baryonic (visible) matter [18, 19]. These two mysterious components are not predicted in the General Relativity (GR). There is two general approaches which can be used to face the DE and DM problems. One could introduce some matter field(s) that affect the dynamics of the evolution of the universe and thereby these observed phenomena may be explained. And, one can alter the geometrical sector of GR to obtain some theoretical results corresponding to the observational ones. In order to apply the former, numerous scenarios have been proposed so far. The cosmological constant can be accounted for the most successful and important candidate for the DE which has a constant equation of state (EoS) parameter. The GR theory comprised by the cosmological constant and DM, is called the concordance or the Λ CDM model [20]. In spite of the high consistency of the Λ CDM model with the present observations, it suffers from an important problem; the theoretical value of the DE density is not compatible with the observationally accepted value. Indeed, their values differ about 120 order of magnitude. This problem is called “the cosmological constant problem” [21–24]. The other proposals for the accelerated expansion of the Universe are the dynamical DE models with time-varying EoS e.g., quintessence and phantom models [25–28]. However, these models may also include the other problems, e.g., the “fine tuning” which is a major one by which the quintessence models are afflicted. Another candidate for DE (which this work have focused

* h.shabani@phys.usb.ac.ir

on it) is the Chaplygin gas (CG) which has been introduced to explain the DE phenomenon [29, 30]. Following a perfect fluid, the EoS for this matter is, $p = -K/\rho$ which K is a constant (this case is called standard Chaplygin gas (SCG)). It has been shown that the Chaplygin cosmology can be interpreted as a transition from a DM dominated universe to an accelerated expansion universe with a intermediate phase with “stiff fluid” (which corresponds to a fluid with $p = \rho$) domination [31]. Although, the SCG model can lead to a transition from a decelerated to accelerated expansion, however, it cannot explain the structure formation and it is faced with some problems with the cosmological power spectrum [33, 34]. Consequently, the EoS of the SCG model has been generalized as $p = -K/\rho^{-\alpha}$, to confront the mentioned issues. Note that, the general CG model (GCG) gives rise to an intermediate epoch with the EoS $p = \alpha\rho$ [30]. The GCG model has been used in the different areas such as, the DE problem [35, 36], Matter power spectrum [37] and wormholes [38, 39].

The geometrical manipulation of GR is the other approach to aim the solving some problems such as DE and DM. Higher order gravity, specially $f(R)$ gravity, by replacing the Ricci scalar in the Einstein-Hilbert action with some scalar invariants, has drawn a remarkable attention among the other models and theories. The $f(R)$ theories of gravity simply replace a function of the Ricci scalar instead of the Ricci scalar itself, has had successes and failures which has been employed in the different realms of gravity theories [40–44]. As an idea to develop the $f(R)$ gravity, some authors incorporate the matter Lagrangian as non-minimally coupled to the geometrical sector of the action [45–49]. In Ref. [50] a more complete form of these type of models titled as $f(R, L_m)$ gravity, proposed. Another suggestion to couple the matter sector to the geometrical one is using the trace of the energy-momentum tensor. This model was presented by authors of Ref. [51], and some others have worked on the various features of it [52–56].

Here, in this work we use both approach, namely, we work on a model in which GCG and the baryonic matter are used as the whole matter in the $f(R, T)$ gravity as the background geometry law. The cosmological consideration of every theory of gravity are based on the investigation of the behavior of the Hubble and the deceleration parameters which are defined by the first and the second order of time derivative of the scale factor, $H = \dot{a}/a$, $q = \ddot{a}/(aH^2)$. The former determines the expansion of the Universe and the latter indicates the acceleration/deceleration behavior. The DE models are constructed so as to match them with the observations. To this reason, the most consistent DE models give the same present values of H and q . Therefore, there is some type of degeneracy in the present values, H_0 and q_0 . To face this matter various strategies are invented. The statefinder diagnosis is an efficient tools to discriminate different DE models. The authors of Ref. [59] introduced new cosmological parameters that are constructed by the third order of time derivative of the scale factor which called “statefinder parameters” and denoted by pair $(s \equiv (r - 1)/3(q - 1/2), r \equiv \ddot{a}/(aH^3))$. Since, this tools use the different orders of the scale factor time derivative, it is a geometrical diagnosis. That is, this method can distinguish between DE models that have the same values of H_0 and q_0 , in a higher level. Note that this method can be extended for models with higher degrees of degeneracy. In the statefinder diagnosis tools, The DE models indicated by the (s, r) plane trajectories and in this way one could consider the behavior of different DE models and thus discriminates them. We have mentioned that the Λ CDM model is still good fitted to the observation and therefore the suggested DE models should not be so far from this model. To understand this fact, the difference between the predicted present values s_0 and r_0 of models and the corresponding values of Λ CDM model $(s_0^{(\Lambda CDM)}, r_0^{(\Lambda CDM)})$ is a criteria for distinction of the DE models.

Up to now, different DE models are diagnosed which are mainly of scalar field models, such as Λ CDM and quintessence DE model that are considered in [59, 60] which are accounted for the first papers that introduced the statefinder diagnosis tools, the interacting quintessence models [61, 62], the holographic DE models [63, 64], the holographic DE model in a non-flat universe [65], the phantom model [66], the tachyon model [67] the GCG model [68], the interacting new agegraphic DE model in a flat and a non-flat universe [69, 70].

We plan our investigations as follow: in Sec. II, we start with presenting the action of $f(R, T)$ gravity and obtain the related field equations and a constrain that must be satisfied by the function $f(R, T)$ to guaranty the conservation of the energy. We devote the rest of this section to present the procedure of obtaining the function $f(R, T)$. We get three classes of the $f(R, T)$ function. Class *I* for the SCG model, Class *II* for the GCG model in the high pressure situations and class *III* for the GCG model in the high densities regimes. In Sec. III we introduce the statefinder parameters and obtain them for the three models, and we also obtain some cosmological parameters. In Sec. IV, we present adequate diagrams to show and discuss the cosmological consequences of these three models, and in Sec. V we summarize our results.

II. FIELD EQUATIONS OF $f(R, T)$ GRAVITY AND THE CONSERVATION OF ENERGY-MOMENTUM TENSOR

In this section we present the field equation of $f(R, T)$ theory of gravity and also discuss the conservation of the energy-momentum tensor when two pressureless matter and GCG are taken into account. By including the two forms

of matters, the action of $f(R, T)$ theory of gravity can be written as

$$S = \int \sqrt{-g} d^4x \left[\frac{1}{16\pi G} f(R, T^{(b, G)}) + L^{(\text{total})} \right], \quad (2.1)$$

where we have defined the Lagrangian of the total matter as

$$L^{(\text{total})} \equiv L^{(b)} + L^{(G)}. \quad (2.2)$$

In the above equations $R, T^{(b, G)} \equiv g^{\mu\nu} T_{\mu\nu}^{(b, G)}$, $L^{(b, G)}$ are the Ricci scalar, the trace of the energy-momentum tensor of the pressureless baryonic matter and GCG (which we get these matters as the total one) and the Lagrangian of the total matter, respectively. The superscript b and G stand for the baryonic matter and GCG gas, g is the determinant of the metric and we set $c = 1$. The energy-momentum tensor $T_{\mu\nu}^{(b, G)}$ is defined as the Euler-Lagrange expression of the Lagrangian of the total matter, i.e.,

$$T_{\mu\nu}^{(b, G)} \equiv - \frac{2}{\sqrt{-g}} \frac{\delta [\sqrt{-g}(L^{(b)} + L^{(G)})]}{\delta g^{\mu\nu}}. \quad (2.3)$$

Instead of obtaining the field equations for the action (2.1), it is sufficient that one gains the corresponding field equations of $f(R, T)$ gravity for general trace T and the matter Lagrangian $L^{(m)}$ and solves them using the two forms of matters; namely, the baryonic matter and GCG. If in the action (2.1), the trace $T^{(b, G)}$ and $L^{(\text{total})}$ are replaced by trace T and $L^{(m)}$, respectively, the field equations for $f(R, T)$ gravity are obtained as

$$F(R, T)R_{\mu\nu} - \frac{1}{2}f(R, T)g_{\mu\nu} + (g_{\mu\nu}\square - \nabla_\mu\nabla_\nu)F(R, T) = (8\pi G - \mathcal{F}(R, T))T_{\mu\nu} - \mathcal{F}(R, T)\Theta_{\mu\nu}, \quad (2.4)$$

where

$$\Theta_{\mu\nu} \equiv g^{\alpha\beta} \frac{\delta T_{\alpha\beta}}{\delta g^{\mu\nu}}, \quad (2.5)$$

and, for the sake of convenience, we have defined the following functions for the derivatives with respect to the trace T and the Ricci scalar R

$$\mathcal{F}(R, T) \equiv \frac{\partial f(R, T)}{\partial T} \quad \text{and} \quad F(R, T) \equiv \frac{\partial f(R, T)}{\partial R}. \quad (2.6)$$

Assuming a perfect fluid and a spatially flat Friedmann–Lemaître–Robertson–Walker (FLRW) metric

$$ds^2 = -dt^2 + a^2(t)(dx^2 + dy^2 + dz^2), \quad (2.7)$$

and using equation (2.4), the generalized Friedmann equation for a matter with non-zero pressure, is achieved as

$$3H^2 F(R, T) + \frac{1}{2}(f(R, T) - F(R, T)R) + 3\dot{F}(R, T)H = (8\pi G + \mathcal{F}(R, T))\rho + \mathcal{F}(R, T)p. \quad (2.8)$$

Applying the Bianchi identity to the field equation (2.4) leads to the following constraint for multi perfect fluids

$$\sum_{i=1}^N \dot{\mathcal{F}}_i(R, T)(\rho_i + p_i) - \frac{1}{2}\mathcal{F}_i(R, T)(\dot{p}_i - \dot{\rho}_i) = 0, \quad (2.9)$$

where N is the number of included perfect fluids. Constraint (2.9) for a pressureless matter reduces to

$$\dot{\mathcal{F}}(R, T) = \frac{3}{2}H(t)\mathcal{F}(R, T). \quad (2.10)$$

Equations (2.9) and (2.10) are two constraints that restrict the form of the Lagrangian density $f(R, T^{(b, G)})$ in our case. These constraints guaranty the conservation of the energy-momentum tensor which is imposed by the Bianchi identity¹. Therefore, to obtain the Hubble parameter from equation (2.8), we need to find the functions $f(R, T^{(b, G)})$ that satisfy these constraints.

¹ Briefly, one can recast the field equations in a canonical form similar to **GR**. In this case, all the other terms can be understood as the matter terms, e.g., [57, 58].

Generally, the function $f(R, T^{(b, G)})$ can take an arbitrary form, however, to avoid mathematical complexities we consider a function of the following form

$$f\left(R, T^{(b, G)}\right) = R + h_1\left(T^{(b)}\right) + h_2\left(T^{(G)}\right). \quad (2.11)$$

Using definitions (2.6) we get

$$\begin{aligned} \mathcal{F}_1\left(R, T^{(b, G)}\right) &= \frac{\partial f\left(R, T^{(b, G)}\right)}{\partial T^{(G)}} = h_1'\left(T^{(G)}\right), \\ \mathcal{F}_2\left(R, T^{(b, G)}\right) &= \frac{\partial f\left(R, T^{(b, G)}\right)}{\partial T^{(b)}} = h_2'\left(T^{(b)}\right), \\ F\left(R, T^{(b, G)}\right) &= \frac{\partial f\left(R, T^{(b, G)}\right)}{\partial R} = 1, \end{aligned} \quad (2.12)$$

where the prime denotes a derivative with respect to the argument. Applying the derivatives (2.12) in equation (2.8), gives

$$3H^2 = \sum_{i=1}^2 \left(8\pi G \rho_i + \mathcal{F}_i(\rho_i + p_i) - \frac{1}{2} h_i \right), \quad (2.13)$$

where the summation should be done over all terms corresponding to the two forms of matters. Notice that, hereafter the arguments in $\mathcal{F}_i(R, T^{(b, G)})$, $h_1(T^{(G)})$ and $h_2(T^{(b)})$ will be dropped for simplicity until we restore them for some purposes.

For a perfect fluid with $p = p(\rho)$, the constraint (2.9) using the trace $T = -\rho + 3p(\rho)$ and the conservation equation $\dot{\rho} + 3H(\rho + p) = 0$, could in principle leads to a differential equation (DE) for the function $f(R, T)$. For the expression (2.11) it reads

$$\left(\dot{h}_1 \rho^{(b)} + \frac{1}{2} h_1' \dot{\rho}^{(b)} \right) + \left[\dot{h}_2 (\rho^{(G)} + p^{(G)}) - \frac{1}{2} h_2' (\dot{\rho}^{(G)} - \dot{p}^{(G)}) \right] = 0. \quad (2.14)$$

Therefore, assuming that the two matters are non-interacting ones, we can obtain

$$\dot{h}_1 \rho^{(b)} + \frac{1}{2} h_1' \dot{\rho}^{(b)} = 0, \quad (2.15)$$

$$\dot{h}_2 (\rho^{(G)} + p^{(G)}) - \frac{1}{2} h_2' (\dot{\rho}^{(G)} - \dot{p}^{(G)}) = 0. \quad (2.16)$$

Since, we have $\rho^{(b)} = -T^{(b)}$ for the pressureless matter, the first equation (2.15) gives

$$h_1(T^{(b)}) = C_1^{(b)} \sqrt{-T^{(b)}} + C_2^{(b)}. \quad (2.17)$$

where C_1 and C_2 are integral constants. Now we try to solve equation (2.16) for GCG. The Eos for GCG is written as

$$P^{(G)} = -\frac{A}{\rho^{(G)\alpha}}. \quad (2.18)$$

Equation (2.18) together with the equation of energy conservation $\dot{\rho}^{(G)} + 3H(\rho^{(G)} + p^{(G)}) = 0$ lead to the following solution for GCG

$$\rho^{(G)} = (A + B a^{-3(1+\alpha)})^{\frac{1}{1+\alpha}}, \quad (2.19)$$

where A , α and B are some constant with the condition that $A > 0$ and $\alpha \geq 0$ ². Setting $\rho_0^{(G)} \equiv \rho^{(G)}(a = 1)$, we can rewrite (2.19) in the suitable form

$$\rho^{(G)} = \rho_0^{(G)} \left(K + (1 - K) a^{-3(1+\alpha)} \right)^{\frac{1}{1+\alpha}}, \quad (2.20)$$

² These restrictions come from the GCG sound speed considerations. See, e.g., Ref. [32].

where a is the scale factor and $K \equiv A/\rho_0^{(G)(1+\alpha)}$. For later applications we rewrite (2.20) as

$$\rho^{(G)} = \rho_0^{(G)} u(a; \alpha, K) \quad (2.21)$$

where

$$u(a; \alpha, K) \equiv \left(K + (1 - K)a^{-3(1+\alpha)} \right)^{\frac{1}{1+\alpha}}. \quad (2.22)$$

which $u(1; \alpha, K) = 1$. Note that, the argument $(1; \alpha, K)$ denotes the variation with respect to the scale factor a for constant values of α and K . Substituting equation (2.18) in (2.16) and also using $\dot{\rho}^{(G)} + 3H(\rho^{(G)} + p^{(G)}) = 0$ and $T = -\rho^{(G)} + 3p^{(G)}$, we get

$$2 \frac{h_2''}{h_2'} = \frac{\rho^{(G)} + \alpha p^{(G)}}{(\rho^{(G)} + 3\alpha p^{(G)})(\rho^{(G)} + p^{(G)})}. \quad (2.23)$$

The left hand side of equation (2.23) is in terms of $T^{(G)}$, however, the right hand side is a function of $\rho^{(G)}$ and $p^{(G)}$, which shows that it is not a closed DE. To complete it, the trace of the energy-momentum tensor of GCG can be rewritten as the following form

$$-\rho^{(G)} - 3 \frac{A}{\rho^{(G)} \alpha} = T^{(G)}. \quad (2.24)$$

By solving equation (2.24), in principle, we can obtain the matter density in terms of the GCG trace, and then, substitute it in equations (2.18) and (2.23) to get a closed DE in terms of the pure trace $T^{(G)}$. Unfortunately, this is not a straightforward calculation, since the equation (2.24) has a lot of roots dependent on the value α (equation (2.24) can be problematic when non-integer values of α are included as well). Furthermore, the solutions can get complicated forms such that the differential equation (2.23) may be not solved. However, for the case of the standard Chaplygin gas (SCG), namely, $\alpha = 1$ the solutions are tractable and for the other values we use the approximation methods. Equation (2.24) for $\alpha = 1$ has the following solutions

$$\rho_{\pm}^{(S)} = \frac{1}{2} \left(-T^{(S)} \pm \sqrt{-12A + T^{(S)2}} \right). \quad (2.25)$$

where superscript ‘‘S’’ stands for SCG. Since, $\rho_{-}^{(S)}$ can gets negative values and thus violates the weak energy condition (WEC), we discard it as a not physical motivated solution, and thus consider the solution $\rho_{+}^{(S)}$. By setting $\alpha = 1$ in equation (2.23), and using (2.25) we reach at

$$2 \frac{h_{2,+}''}{h_{2,+}'} = \frac{1}{(2\rho_{+}^{(S)} + T^{(S)})} = \frac{1}{\sqrt{-12A + T^{(S)2}}}, \quad (2.26)$$

and, we finally obtain the following DE

$$2\sqrt{-12A + T^{(S)2}} h_{2,+}'' - h_{2,+}' = 0, \quad (2.27)$$

where the solution $h_{2,+}$ is corresponding to $\rho_{+}^{(S)}$. The solutions of the above DE is

$$h_{2,+}(T^{(S)}) = -\frac{2}{3} C_{1+}^{(S)} \left(-2T^{(S)} + \sqrt{-12A + T^{(S)2}} \right) \sqrt{T^{(S)} + \sqrt{-12A + T^{(S)2}}} + C_{2+}^{(S)}, \quad (2.28)$$

where $C_{1+}^{(S)}$ and $C_{2+}^{(S)}$ are constants of integration. As a result, in the $f(R, T)$ theory of gravity, for the non-interacting baryonic matter and SCG matters, the conservation of the energy-momentum tensor enforce us to use the following function

$$f^{(I)}(R, T^{(m, S)}) = R + C_1^{(b)} \sqrt{-T^{(b)}} - \frac{2}{3} C_1^{(S)} \left(-2T^{(S)} + \sqrt{-12A + T^{(S)2}} \right) \sqrt{T^{(S)} + \sqrt{-12A + T^{(S)2}}} + \Lambda_1^{(b, S)} \quad (2.29)$$

where we have restored the argument of function f for clarification and dropped the sign ‘‘+’’. Also, we have added the superscript I for later applications and $\Lambda_1^{(b, G)} \equiv C_2^{(b)} + C_2^{(S)}$. Nevertheless, we consider two another model; the

models which use GCG in two extreme situations, when $p^{(G)} \gg \rho^{(G)}$ and $\rho^{(G)} \gg p^{(G)}$. These cases will be considered for arbitrary values of α . In either cases we approximate $T_p^{(G)} \simeq 3p^{(G)} = -3|p^{(G)}|$ and $T_\rho^{(G)} \simeq -\rho^{(G)}$. In these cases, using equation (2.16), the related DE's are given as

$$2T_p^{(G)}h_{2,p}''(T_p^{(G)}) - h_{2,p}'(T_p^{(G)}) \simeq 0, \quad (2.30)$$

$$2T_\rho^{(G)}h_{2,\rho}''(T_\rho^{(G)}) + h_{2,\rho}'(T_\rho^{(G)}) \simeq 0, \quad (2.31)$$

with the solutions

$$h_{2,p}(T_p^{(G)}) = \frac{2}{3}C_{1p}^{(G)} \left(-T^{(G)}\right)^{3/2} + C_{2p}^{(G)}, \quad (2.32)$$

and

$$h_{2,\rho}(T_\rho^{(G)}) = 2C_{1\rho}^{(G)} \sqrt{-T^{(G)}} + C_{2\rho}^{(G)}, \quad (2.33)$$

where we have again restored the arguments and labeled the equations and solutions by p and ρ denoting the either extreme cases and $C_{ip}^{(G)}$ and $C_{i\rho}^{(G)}$ with $i = 1, 2$ are integral constants. Thus, we have two another forms of $f(R, T)$ function, i.e.,

$$f^{(II)}(R, T^{(b, G)}) = R + C_1^{(b)} \sqrt{-T^{(b)}} + \frac{2}{3}C_{1p}^{(G)} \left(-T^{(G)}\right)^{3/2} + \Lambda_p^{(b, G)} \quad (2.34)$$

for $|p^{(G)}| \gg \rho^{(G)}$, where $\Lambda_p^{(b, G)} \equiv C_2^{(b)} + C_{2p}^{(G)}$ and

$$f^{(III)}(R, T^{(b, G)}) = R + C_1^{(b)} \sqrt{-T^{(b)}} + 2C_{1\rho}^{(G)} \sqrt{-T^{(G)}} + \Lambda_\rho^{(b, G)} \quad (2.35)$$

for $\rho^{(G)} \gg |p^{(G)}|$, where $\Lambda_\rho^{(b, G)} \equiv C_2^{(b)} + C_{2\rho}^{(G)}$. Note that, there is two sets of constants labeled by the numbers 1 and 2 which determine the degree of involved DE's.

Therefore, we have three non-interacting models including pressureless baryonic matter and three forms of Chaplygin gas; in the first one we have SCG represented by the function (2.29), the second one is GCG when the matter density is negligible with respect to the pressure shown by the function (2.34), and in the last case the matter density is dominant determined by the function (2.35).

Note that, from equations (2.18) and (2.20), the EoS parameter $w^{(GCG)}$ for the GCG matter can be obtained. At the early time ($a \rightarrow 0$), we have $w^{(GCG)} \rightarrow 0$, and at the late time ($a \rightarrow \infty$), $w^{(GCG)} \rightarrow -1$. It means that the GCG matter in the early time behaves like DM and in the early time like DE. Therefore, we assume that DE and DM are unified by GCG model. And besides, we have the baryonic matter indicated by superscript (m) which does not interact with GCG component.

In the next section, we present statefinder parameters and obtain them for these three models, and get the deceleration parameter and define the effective EoS, as well. Henceforth, we will call these as, models I, II and III.

III. STATEFINDER PARAMETERS AND THE RELATED DEFINITIONS

In this section, we present the definitions of the statefinder parameters and calculate them for the models *I*, *II* and *III*. These parameters are important to discuss the cosmological aspects of models. The statefinder parameters are defined via the following pairs of parameters

$$r \equiv \frac{\ddot{a}}{a} H^{-3}, \quad (3.1)$$

$$s \equiv \frac{r - 1}{3(q - 1/2)}. \quad (3.2)$$

models that have the same present values of the Hubble parameter H_0 , and the deceleration parameter q_0 , can be discriminated by these parameters from each other. These parameters include the third time derivative of the scale factor (in spite of the Hubble parameter which includes the first time derivative and the deceleration parameter which

include the second time derivative of the scale factor) and can be used to discriminate the different DE models. The deceleration parameter is defined as the first time derivative of the Hubble parameter, i.e.,

$$q \equiv -\frac{\dot{H}}{H^2} - 1, \quad (3.3)$$

which in terms of the normalized Hubble parameter $E(a) = H/H_0$, it can be rewritten as

$$q = -\frac{1}{E} \frac{dE}{dN} - 1, \quad (3.4)$$

where $N \equiv \ln a$. Using the definition (3.3), the statefinder parameter r can be simply calculated as

$$r = q(1 + 2q) - \frac{dq}{dN}, \quad (3.5)$$

which substituting (3.4) in (3.5) gives

$$r = \frac{1}{E} \frac{d^2 E}{dN^2} + \frac{1}{E^2} \left(\frac{dE}{dN} \right)^2 + \frac{3}{E} \frac{dE}{dN} + 1. \quad (3.6)$$

One can use equations (3.5) and (3.6), to obtain the statefinder parameter s from definition (3.2). According to the definition of the normalized Hubble parameter, and also using (2.13) for the models (2.29), (2.34) and (2.35) we obtain

$$E^{(I)}(a; 1, K) = \left[\Omega_0^{(b)} \left(1 - \mathbf{m}a^{3/2} \right) a^{-3} + \Omega_0^{(S)} u(a; 1, K) \left(1 - \sqrt{24} \mathbf{n}^{(I)} \left(\frac{u(a; 1, K)}{K} \right)^{-3/2} \right) \right]^{\frac{1}{2}}, \quad (3.7)$$

$$E^{(II)}(a; \alpha, K) = \left[\Omega_0^{(b)} \left(1 - \mathbf{m}a^{3/2} \right) a^{-3} + \Omega_0^{(G)} u(a; \alpha, K) \left(1 - \sqrt{12} \mathbf{n}^{(II)} K^{\frac{3}{2}} u(a; \alpha, K)^{-\frac{3\alpha+2}{2}} \right) \right]^{\frac{1}{2}} \quad (3.8)$$

and

$$E^{(III)}(a; \alpha, K) = \left[\Omega_0^{(b)} \left(1 - \mathbf{m}a^{3/2} \right) a^{-3} + \Omega_0^{(G)} u(a; \alpha, K) \left(1 - 2 \mathbf{n}^{(III)} u(a; \alpha, K)^{-\frac{1}{2}} \right) \right]^{\frac{1}{2}} \quad (3.9)$$

where we have defined the density parameters for the two type of matters and some dimensionless parameters, as

$$\Omega_0^{(b)} = \frac{8\pi G \rho_0^{(b)}}{3H_0^2}, \quad \Omega_0^{(S)} = \frac{8\pi G \rho_0^{(S)}}{3H_0^2}, \quad \mathbf{m} = \frac{\rho_0^{(b)-1/2} C_1^{(b)}}{8\pi G}, \quad (3.10)$$

$$\mathbf{n}^{(I)} = \frac{\rho_0^{(S)1/2} C_1^{(S)}}{8\pi G}, \quad \mathbf{n}^{(II)} = \frac{\rho_0^{(G)1/2} C_{1p}^{(G)}}{8\pi G}, \quad \mathbf{n}^{(III)} = \frac{\rho_0^{(G)-1/2} C_{1\rho}^{(G)}}{8\pi G}. \quad (3.11)$$

Hence, each model involved some parameters; the space parameters of the model *I* are $(\mathbf{m}, \mathbf{n}^{(I)}, K)$, those of the model *II* are $(\mathbf{m}, \mathbf{n}^{(II)}, K, \alpha)$ and for the model *III* we have $(\mathbf{m}, \mathbf{n}^{(III)}, K, \alpha)$. These parameters play the role of some tuners for these models which can be set for a physically interesting situation. From equations (3.4), (3.7), (3.8) and (3.9), the deceleration parameter are obtained as

$$q^{(I)} = \frac{3}{4E^{(I),2}} \left[\Omega_0^{(b)} (2 - \mathbf{m}a^{3/2}) a^{-3} + 2\Omega_0^{(S)} (1 - K) uv \left(1 + \sqrt{6} \mathbf{n}^{(I)} (u/K)^{-3/2} \right) \right] - 1, \quad (3.12)$$

$$q^{(II)} = \frac{3}{4E^{(II),2}} \left[\Omega_0^{(b)} (2 - \mathbf{m}a^{3/2}) a^{-3} + 2\Omega_0^{(G)} (1 - K) v \left(u + \sqrt{27} \alpha \mathbf{n}^{(II)} \left(\frac{u^\alpha}{K} \right)^{-3/2} \right) \right] - 1, \quad (3.13)$$

$$q^{(III)} = \frac{3}{4E^{(III),2}} \left[\Omega_0^{(b)} (2 - \mathbf{m}a^{3/2}) a^{-3} + 2\Omega_0^{(G)} (1 - K) uv \left(1 - \mathbf{n}^{(III)} u^{-\frac{1}{2}} \right) \right] - 1 \quad (3.14)$$

for the models *I*, *II* and *III*, respectively. It is convenient to define an effective EoS in the higher order gravity (specially in $f(R)$ gravity) to explain the present accelerated expansion of the Universe through the effects of the geometrically modified gravity terms in the Friedmann equations³. Here, we have not included the modifications in the geometrical sector of the action, however, there is a non-standard interaction between cosmological fluids and normal geometrical sector, which is the general behavior of $f(R, T)$ gravity. The effective EoS parameter $w^{(\text{eff})}$ is defined as $w^{(\text{eff})} = -1 - 2\dot{H}/3H^2$, which using the definition (3.3) reads,

$$w^{(\text{eff})} = \frac{1}{3}(2q - 1), \quad (3.15)$$

which it can be obtained for the three models from (3.12), (3.13) and (3.14). The statefinder parameters r and s are calculated as

$$r^{(I)} = \frac{9}{8E^{(I),2}} \left\{ \Omega_0^{(b)} \mathbf{m} a^{-3/2} + \Omega_0^{(S)} (1-K) u^{-1} v \left[4K + \sqrt{24} \mathbf{n}^{(I)} \left(2 - 5(1-K)v \right) (u/K)^{-3/2} u^2 \right] \right\} + 1, \quad (3.16)$$

$$r^{(II)} = \frac{9}{8E^{(II),2}} \left\{ \Omega_0^{(b)} \mathbf{m} a^{-3/2} + 2\alpha \Omega_0^{(G)} (1-K)v \left[2 \left(1 - (1-K)v \right) u + \sqrt{27} \mathbf{n}^{(II)} \left(2\alpha - (1-K)(2+5\alpha)v \right) \left(\frac{u^\alpha}{K} \right)^{-3/2} \right] \right\} + 1, \quad (3.17)$$

$$r^{(III)} = \frac{9}{8E^{(III),2}} \left\{ \Omega_0^{(b)} \mathbf{m} a^{-3/2} + 2\Omega_0^{(G)} (1-K)vu \left[2\alpha \left(1 - (1-K)v \right) - \mathbf{n}^{(III)} \left(2\alpha - (1-K)(1+2\alpha)v \right) u^{-\frac{1}{2}} \right] \right\} + 1, \quad (3.18)$$

and

$$s^{(I)} = \frac{1}{2} \frac{\Omega_0^{(b)} \mathbf{m} a^{-3/2} + \Omega_0^{(S)} (1-K) u^{-1} v \left[4K + \sqrt{24} \mathbf{n}^{(I)} \left(2 - 5(1-K)v \right) (u/K)^{-3/2} u^2 \right]}{\Omega_0^{(b)} \mathbf{m} a^{-3/2} - \Omega_0^{(S)} u^{-1} \left[2K - \sqrt{24} \mathbf{n}^{(I)} \left(2 + (1-K)v \right) (u/K)^{-3/2} u^2 \right]}, \quad (3.19)$$

$$s^{(II)} = \frac{1}{2} \frac{\Omega_0^{(b)} \mathbf{m} a^{-3/2} + 2\alpha \Omega_0^{(G)} (1-K)v \left[2 \left(1 - (1-K)v \right) u + \sqrt{27} \mathbf{n}^{(II)} \left(2\alpha - (1-K)(2+5\alpha)v \right) \left(\frac{u^\alpha}{K} \right)^{-\frac{3}{2}} \right]}{\Omega_0^{(b)} \mathbf{m} a^{-3/2} - \Omega_0^{(G)} \left[2 \left(1 - (1-K)v \right) u - \sqrt{12} \mathbf{n}^{(II)} \left(2 + 3\alpha(1-K)v \right) \left(\frac{u^\alpha}{K} \right)^{-\frac{3}{2}} \right]}, \quad (3.20)$$

$$s^{(III)} = \frac{1}{2} \frac{\Omega_0^{(b)} \mathbf{m} a^{-3/2} + 2\Omega_0^{(G)} (1-K)vu \left[2\alpha \left(1 - (1-K)v \right) - \mathbf{n}^{(III)} \left(2\alpha - (1-K)(1+2\alpha)v \right) u^{-\frac{1}{2}} \right]}{\Omega_0^{(b)} \mathbf{m} a^{-3/2} - 2u\Omega_0^{(G)} \left[1 - (1-K)v - \mathbf{n}^{(III)} \left(2 - (1-K)v \right) u^{-\frac{1}{2}} \right]}. \quad (3.21)$$

where we have defined $v(a; \alpha, K) = [a^3 u(a; \alpha, K)]^{-(1+\alpha)}$, and also dropped the arguments $(a; 1, K)$ and $(a; \alpha, K)$ from the parameters of the models *I* and the two other ones, respectively. Note that, the dimensionless parameters (3.10)

³ For example, see Ref. [71] and references therein.

are not independent. Applying the present value $E_0^{(I)}(1; \alpha, K) = 1$, and also the same for the other models, gives

$$\Omega_0^{(S)} = \frac{1 - (1 - m)\Omega_0^{(b)}}{1 - \sqrt{12}n^{(I)}K^{\frac{3}{2}}} \quad \text{for model } I, \quad (3.22)$$

$$\Omega_0^{(G)} = \frac{1 - (1 - m)\Omega_0^{(b)}}{1 - \sqrt{24}n^{(II)}K^{\frac{3}{2}}} \quad \text{for model } II, \quad (3.23)$$

$$\Omega_0^{(G)} = \frac{1 - (1 - m)\Omega_0^{(b)}}{1 - 2n^{(III)}} \quad \text{for model } III. \quad (3.24)$$

Setting $\mathbf{m} = 0$ and $\mathbf{n}'s = 0$, in the equations (3.12)-(3.21), gives the corresponding equations for the model $f(R, T) = R$. These coupling constants are responsible for all deviations of the above equations from the equivalent forms in GR. In the next section we consider these deviations for three models *I*, *II* and *III*, numerically. That is, we investigate the cosmological consequences of equations (3.12)-(3.21) through the statefinder diagnosis.

IV. STATEFINDER DIAGNOSIS AND NUMERICAL CONSIDERATIONS

In this section we consider equations (3.12)-(3.21) and extract their cosmological consequences via the statefinder diagnosis. These three models depend on the coupling constants \mathbf{m} and $\mathbf{n}'s$, and also the constant K for the model *I*, and K, α for the two other ones. Generally, these constants can lead to different models for different values, and therefore, different cosmological history for the universe. In the following subsections we consider each model, in turn.

Note that, in each forthcoming diagram, the cosmological parameters curves for $\mathbf{m}, \mathbf{n}'s = 0$ corresponds to the GR background. Namely, one can compare the $f(R, T)$ gravity results to the corresponding GR ones in each model *I*, *II*, and *III*, using these plots.

A. The model $f^{(I)}(R, T^{(b, S)})$

Using equations (3.12) and (3.15), the cosmological evolution of the EoS parameter for this model is illustrated in Fig. 1, for specific values $K = 0, 0.33, 0.77$ and 0.99 with $\mathbf{m}, \mathbf{n}^{(I)} = -1$. Moreover, we have plotted the corresponding diagrams for the standard case $\mathbf{m} = 0, \mathbf{n}^{(I)} = 0$ (i.e., for GR, as we have before mentioned) to indicate the possible deviations. The zero value for K , corresponds to the model with the pressureless matter (see equation (2.20)), and the other values determine different cosmological scenarios. The predicted present value $w_0^{(\text{eff})}$, indicated by a solid circle on each curve. Brown dashed line used for case $K = 0$, blue dotted one for $K = 0.33$, red dotted-dashed curve show the case $K = 0.77$ and a black line used for the models with $K = 0.99$ ⁴. Since, there generally is some divergency in the cases with positive values of $\mathbf{n}^{(I)}$ and \mathbf{m} (in a certain value of N , for some values of K), the evolution of the related EoS parameter are not depicted in Fig. 1. Also, this divergency causes a total increase in the value of the deceleration parameter after the matter dominated era. Hence, the positive values for the coupling constants $\mathbf{m}, \mathbf{n}^{(I)}$, can lead to non-physical behaviors, and we discard such cases as the less physical interested ones⁵. However, one may find some curves without divergency for the positive values. Plots in Fig. 1 show that the value of the effective EoS are much more near to its observationally obtained values, $w_0^{(\text{obs})} \simeq -1$ [] for $\mathbf{n}^{(I)} \neq 0$. For example, for $\mathbf{m} = 2, \mathbf{n}^{(I)} = -2.3$ and $K = 0.32$ we can obtain the acceptable value $w_0^{(\text{eff})} \simeq -1.005$, consistent with the recent results [?]. Decreasing the parameter $\mathbf{n}^{(I)}$ for $\mathbf{m} = 0$, leads to smaller values of $w_0^{(\text{eff})}$ for all values of K . By contrast, decreasing in the parameter \mathbf{m} for $\mathbf{n}^{(I)} = 0$, gives smaller values for $K < 1/2$ and larger values for $K > 1/2$. To understand the reason of this dual behavior, we calculate the present value of $w_0^{(\text{eff})}$ for $\mathbf{n}^{(I)} = 0$ as

$$w_0^{(\text{eff})} = K(\Omega_0^{(b)} - 1) - \frac{1}{2}(2K - 1)\mathbf{m}\Omega_0^{(b)}, \quad \mathbf{n}^{(I)} = 0, \quad N = 0. \quad (4.1)$$

As one can see, for special case $K = 1/2$, the effective EoS is independent of the parameter \mathbf{m} and for a given \mathbf{m} , the value of $w_0^{(\text{eff})}$ increases for $K > 1/2$ and decreases for $K < 1/2$. Calculations show that when $\mathbf{n}^{(I)} \neq 0$, the mutual behavior is absent and in these situations a decrease in \mathbf{m} leads to an increase in $w_0^{(\text{eff})}$ for all values of K (compare

⁴ In the subsequent discussions and subsections we always use these options to show the related plots for $K = 0, 0.33, 0.77, 0.99$.

⁵ Note that, to these reasons, we do not consider the other cosmological parameters for this model and also for two other ones for the positive valued parameters $\mathbf{m}, \mathbf{n}'s$.

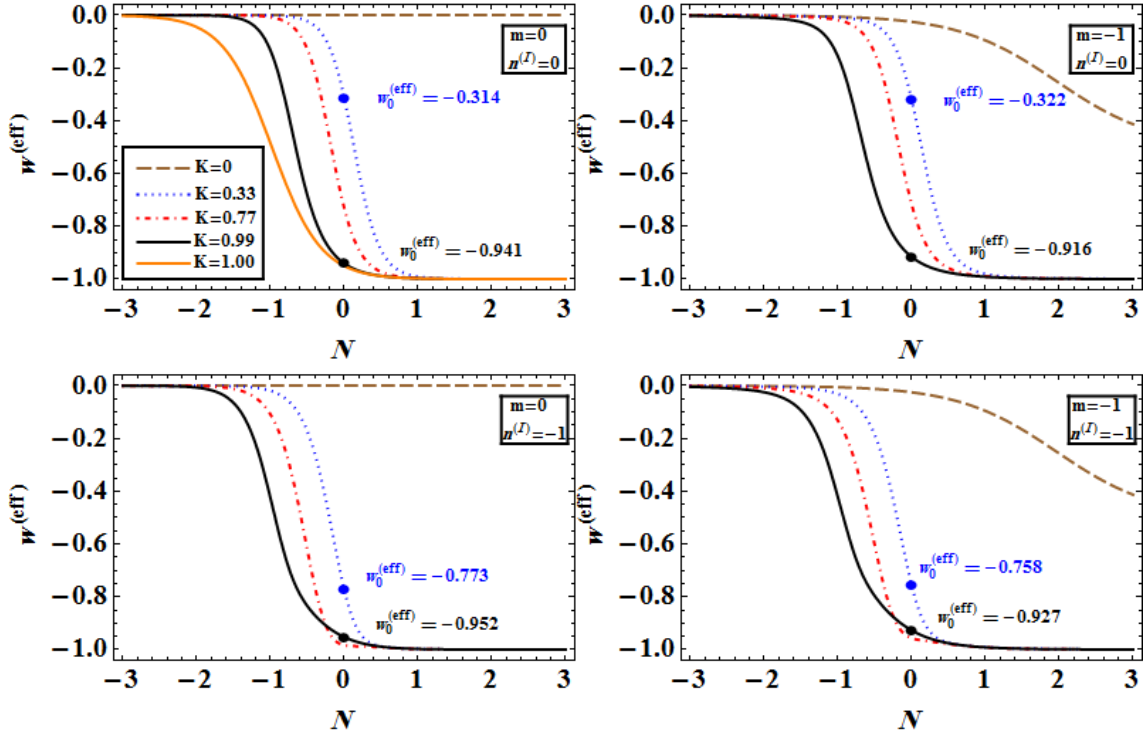


Figure 1. (color online). The cosmological evolution of the effective equation of state (EoS) parameter of model I versus $N \equiv \ln a$, where a is the scale factor the Universe. The curves are plotted for $K = 0$ (indicated the dark matter (DM) in addition to the baryonic one) in brown dashed line, blue dotted line for $K = 0.33$, red dotted-dashed line for case $K = 0.77$, black solid line for $K = 0.99$ and orange solid one for $K = 1.00$. Since, positive values of parameters \mathbf{m} and $\mathbf{n}^{(I)}$ lead to some abnormality, only negative values are discussed. The curve of $K = 1.00$ is not flat because of the effect of the baryonic matter density. Zero value for the coupling constants \mathbf{m} and $\mathbf{n}^{(I)}$ reflects the GR background. Columnar view shows that decreasing the value of $\mathbf{n}^{(I)}$ leads to decreasing the present values. However, lateral view demonstrate that decreasing \mathbf{m} leads to an increase for $K > 0.5$ and a decrease for $K < 0.5$. And, an orthogonal look shows that the overall effect of switching on both parameter leads to more observationally accepted values for $K < 0.5$. For, larger values of \mathbf{m} and $\mathbf{n}^{(I)}$ we get the better results.

below diagrams in Fig. 1). Therefore, in lower right diagram we see a total decrease in the value of $w_0^{(\text{eff})}$ (a decrease for the effect of $\mathbf{n}^{(I)} \neq 0$ and an increase for the effect of \mathbf{m}). The value of $w_0^{(\text{eff})}$ vanishes in the early times ($N < 0$ which corresponds to $a < 1$), and goes to -1 in the late times except for the case $K = 0$. However, for models with $\mathbf{m} \neq 0$ this does not occurs (see right panels in Fig. 1).

The evolution of the deceleration parameter (3.12), is presented in Fig. 2. An interesting result is that, the value of the deceleration parameter for the models with $K = 0$, is running when $\mathbf{m} < 0$. The curve corresponding to $K = 0$, is sensitive to the negative values of \mathbf{m} . Plots show that, there is a transition between the value $1/2$ and the negative values of q . This transition for $K = 0$ is relatively slower than for the other value of K ; the larger values the parameter \mathbf{m} gets, the later the transition occurs. In addition to the mentioned effect of the negative values of \mathbf{m} for curves with $K = 0$, the overall effects of the parameters \mathbf{m} and \mathbf{n} can be distinguished. To this end, the present values of the deceleration function q_0 in Fig. 2, and the statefinder parameters r_0 and s_0 in Fig. 3, are specified for some curves. Comparing upper left corner diagram with lower left one in Fig. 2, show that the net effect of $\mathbf{n}^{(I)} (< 0)$ is decreasing the values of q_0 . Since, there is a linear relation between the deceleration and EoS parameters, there exists a similar mutual behavior for the effect of \mathbf{m} .

In Fig. 3, the evolution of the statefinder parameters in the (s, r) plane for $K = 0.33, 0.77, 0.99$ are presented. In this plane, the values of s mapped on a horizontal axis and a vertical axis determine the values of r . In left upper corner, we plot the diagrams held for GR, to see the possible deviations. In each panel besides the present values (which are indicated by small solid point), we represent starting point with a star symbol (corresponding to a point in the early times), the position of the Λ CDM model (corresponding to future) with a solid small box and the direction of the evolution of the trajectories with the colored arrows. The starting point correspond to the early times indicated

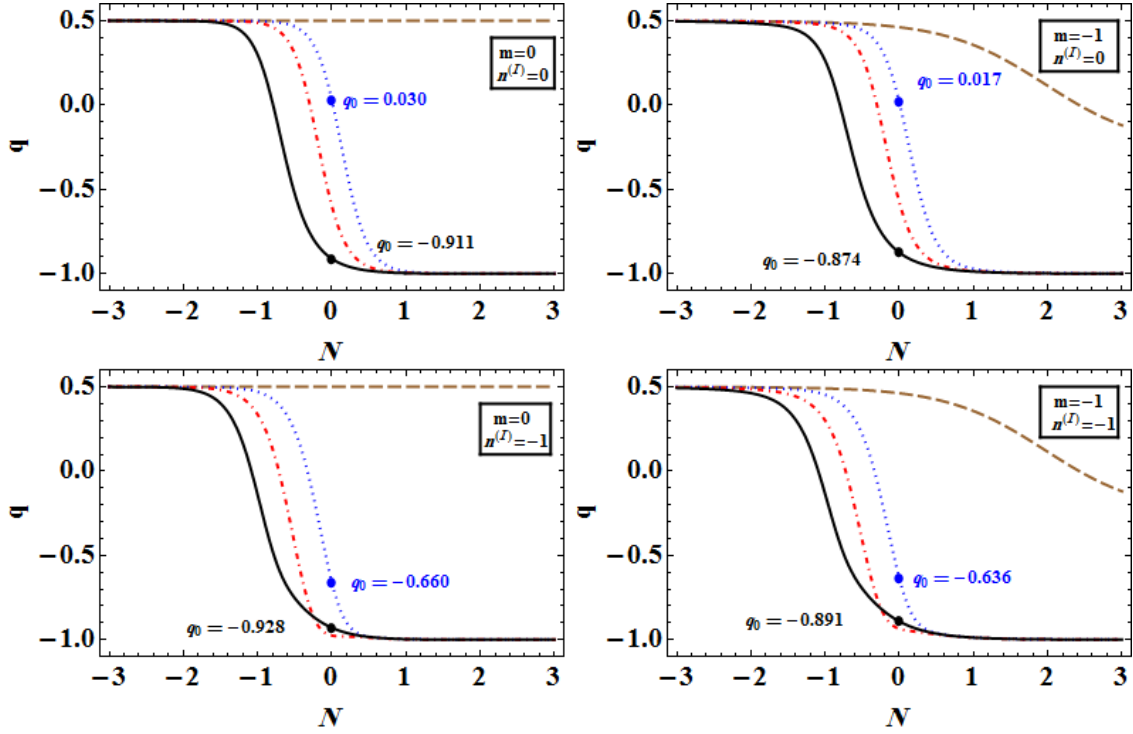


Figure 2. (color online). The evolution of the deceleration parameter of model I for different negative values of the parameters K , \mathbf{m} and $\mathbf{n}^{(I)}$. The curves are plotted for $K = 0$, $K = 0.33$, $K = 0.77$ and $K = 0.99$ corresponding to brown dashed line, blue dotted line for, red dotted-dashed line and black solid line. All diagrams are drawn for the present baryonic matter density $\Omega_0^{(b)} = 0.05$. The case $K = 0$ corresponds to the presence of only the baryonic and CDM. In this case, the deceleration parameter is constant 0.5 in GR (corresponds to $\mathbf{m}, \mathbf{n}^{(I)} = 0$), on the contrary, decreasing the value of \mathbf{m} , leads to the deceleration parameter varies in $f(R, T)$ gravity. By decreasing both parameters, we obtain the better results for the only cases with $K < 0.5$, however, decreasing in $\mathbf{n}^{(I)}$ improves the result for all values $0 < K < 1$.

by the condition $a \rightarrow 0$. In the limit $a \rightarrow 0$, the statefinder parameter r reads

$$r^{(I)}(a \rightarrow 0) = 1 + \frac{9\mathbf{m}\Omega_0^{(m)}a^{3/2}}{8\left(\Omega_0^{(m)} - \frac{\sqrt{1-K}(1+(\mathbf{m}-1)\Omega_0^{(m)})}{2\sqrt{6}K^{3/2}\mathbf{n}^{(I)}-1}\right)}, \quad (4.2)$$

accordingly, in the early times $a \rightarrow 0$, we obtain $r = 1$. However, the limit of s for $a \rightarrow 0$ depends on the value of the parameters \mathbf{m} and $\mathbf{n}^{(I)}$; for zero value for the both we have $s = -1$, if only the former is vanished $s = -1/2$, and otherwise we have $s = +1/2$. Therefore, for non-interacting SCG and baryonic matters, in the background of $f(R, T)$ theory of gravity, the trajectories of the statefinder plane belongs to three different classes; some trajectories have the initial value ($s = -1, r = 1$), and two other class with ($s = \pm 1/2, r = 1$), as the initial values. However, all trajectories terminate at the Λ CDM fixed point, since the statefinder parameters in the limit $a \rightarrow \infty$ take the following forms

$$r^{(I)}(a \rightarrow \infty) = 1 + \mathcal{C}_1\left(K, \mathbf{m}, \mathbf{n}^{(I)}, \Omega_0^{(m)}\right)a^{-3/2} \quad (4.3)$$

$$s^{(I)}(a \rightarrow \infty) = \mathcal{C}_2\left(K, \mathbf{m}, \mathbf{n}^{(I)}, \Omega_0^{(m)}\right)a^{-3/2}. \quad (4.4)$$

Here, in model I , there are different scenarios for the evolution of the Universe, with more or less the same feature in their deceleration parameters, but completely different feature in the (r, s) plane; the Universe begins with different initial points, however, terminates in the same point in the late times, mimicking the cosmological constant. Lateral comparison of diagrams in Fig. 3, show that for a specific value of K , the net effect of negative values of \mathbf{m} is an increasing in the value of s_0 , and a decreasing in the value of r_0 . And a columnar view, show that negative values of $\mathbf{n}^{(I)}$ increase the value of s_0 . Nevertheless, in these cases the value of r_0 are increased for $0.17 < K < 0.33$ (the maximum value $r_{0,max} \simeq 1.76$ occurs in $K \simeq 0.24$), and decreased otherwise. Diagonal comparison demonstrate that the distance to the Λ CDM fixed point is shorter when both parameters \mathbf{m} and $\mathbf{n}^{(I)}$ are turned on. This effect is more effective for large K ; for $K \rightarrow 1$ one obtains similar result to solutions (4.3). Thus, all trajectories with the property $K \rightarrow 1$, terminate at the Λ CDM fixed point. This characteristics is also reported in [?]

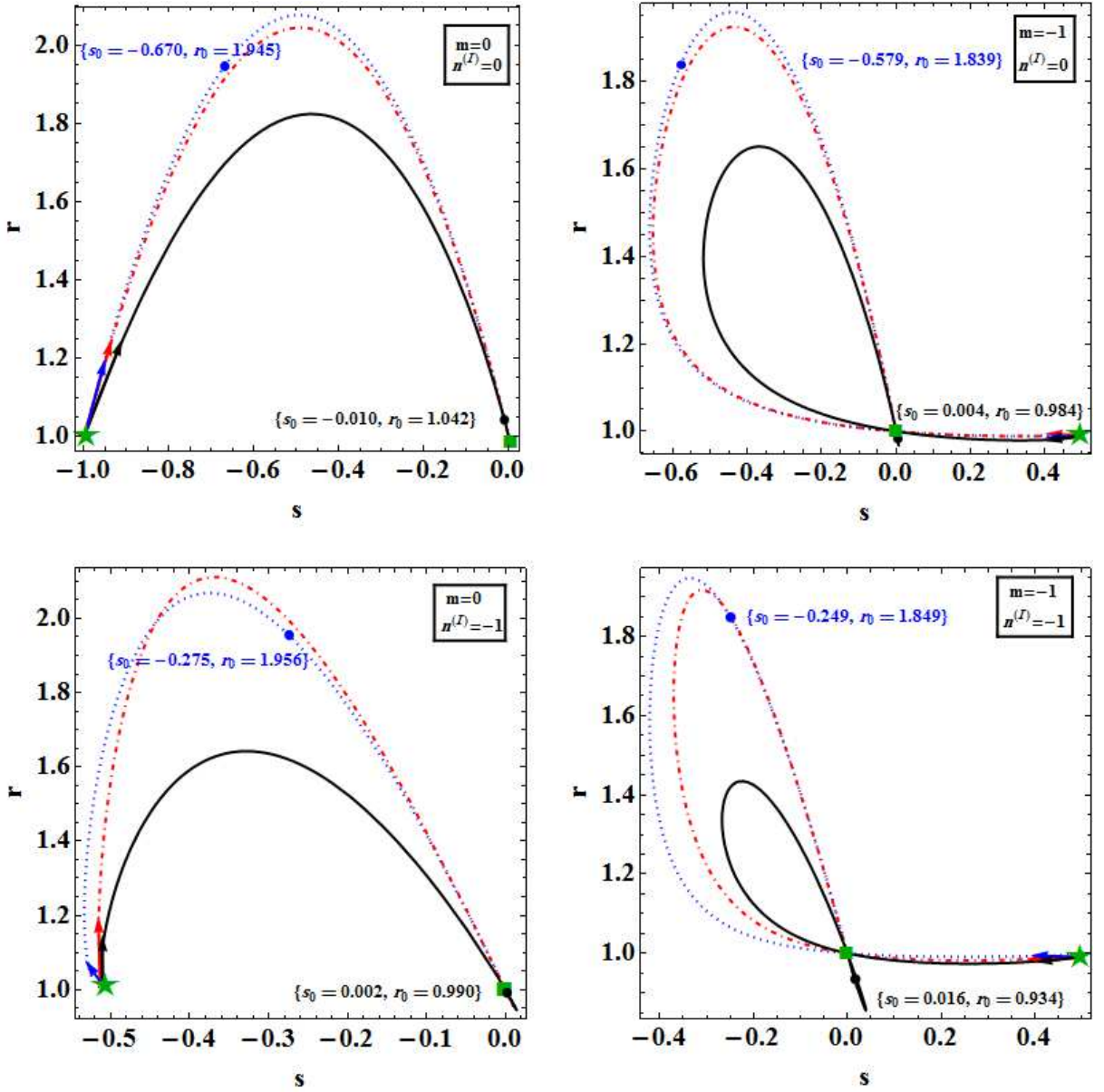


Figure 3. (color online). Statefinder diagnosis of model *I* in the (s, r) plane. In this plane the parameter r corresponds to the vertical axis and the values of parameter s form the horizontal axis. Each trajectory start from a star symbol and end up at a boxed symbol. the star symbol denotes the initial value for the trajectories. There is three different cases; some trajectories start from $(-1, 1)$ (left upper corner), some start from $(-0.5, 1)$ (left lower corner) and other trajectories begins from $(+0.5, 1)$ (right diagrams). However, all trajectories terminate at the boxed symbol place with coordinate $(0, 1)$ which belongs to the Λ CDM model. The diagram in right lower corner shows that decreasing the values of \mathbf{m} and $\mathbf{n}^{(I)}$ reduces the distance to the Λ CDM fixed point which for $K > 0.5$ is more effective.

B. The model $f^{(II)}(R, T^{(b, G)})$

In this model besides the model coupling constants $\mathbf{m}, \mathbf{n}^{(II)}$ and the parameter K , there is another parameter, α , as the fourth constant. Therefore, the net effects of this parameter should be considered. The related figures of the effective EoS parameter $w^{(\text{eff})}$, for this model are illustrated in Fig. 4. Again, the curves for $K = 0, 0.33, K = 0.77$ and $K = 0.99$, corresponding to brown dashed, blue dotted, red dotted-dashed and black solid lines are plotted, respectively. Here, the diagrams for $\alpha = 0.001, 0.99$ are drawn. It is clear from equations (3.7), (3.8), (3.9) and (3.12), (3.13), (3.14), that the deceleration and accordingly the effective EoS parameters are the same for models *I*, *II* and *III*, when $\mathbf{n} = 0$'s go to zero. Hence, in this case the diagrams for $w^{(\text{eff})}$ and q are not redrawn in model(s) *II* (and *III* in the later subsection). We arrange the diagrams the same as model *I*, however in this case the parameter α

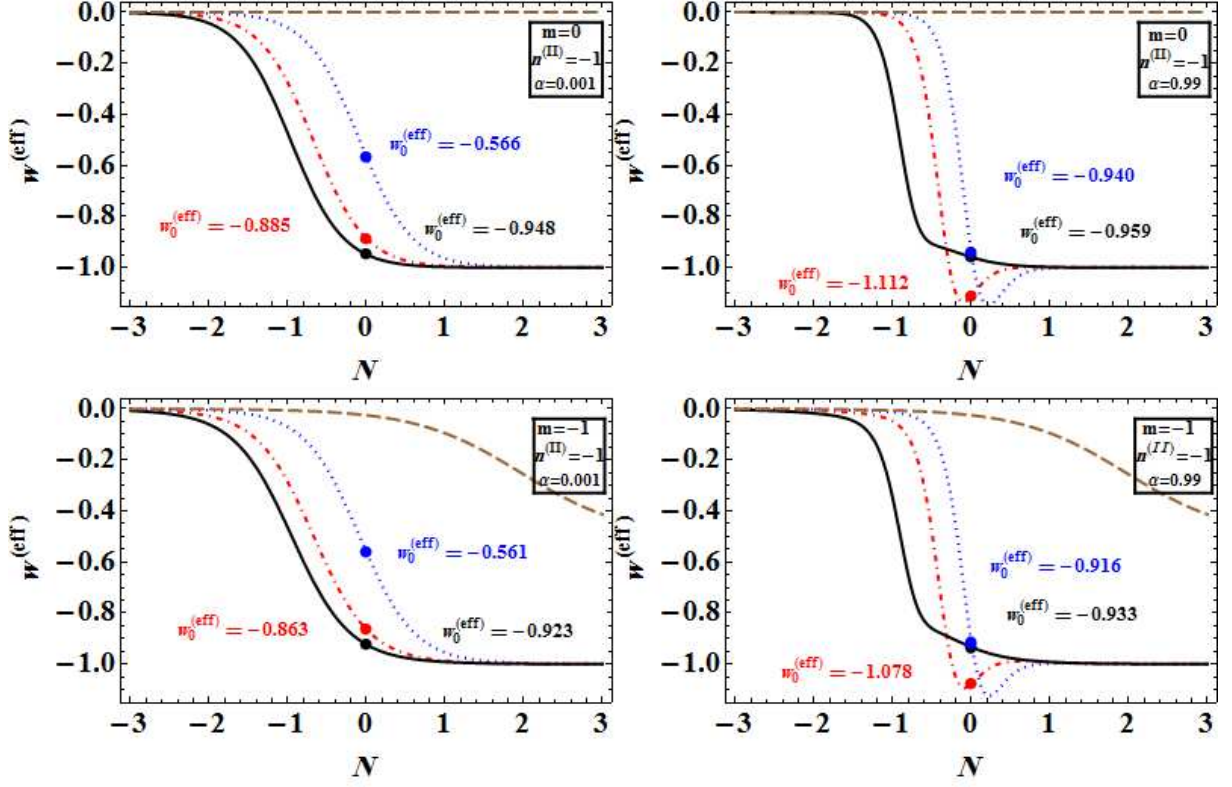


Figure 4. (color online). The evolution of the effective EoS parameter for non-interacting baryonic matter with the GCG matter in the high pressure regime, model *II*. The curves are plotted for $K = 0$ (brown dashed line), $K = 0.33$ (blue dotted line), $K = 0.77$ (red dotted-dashed line) and $K = 0.99$ (black solid line), for $\mathbf{m} = 0, -1$, $\mathbf{n}^{(II)} = -1$ and $\alpha = 0.001, 0.99$. The present values are also depicted with the corresponding colors. An increase in the value of α , decreases the value of $w_0^{(\text{eff})}$.

increase horizontally. An increase in the value of α leads to a decrease in the value of $w_0^{(\text{eff})}$, and this affects on the relatively smaller values of K , strongly. In this model we obtain more acceptable results in all range $0 < \alpha < 1$; left upper diagram shows that even for $\alpha = 0.001$ we have $w_0^{(\text{eff})} \simeq -0.9$ (red dotted-dashed line), the result that met in model *I* only for $K \rightarrow 1$. By comparing the effective EoS diagrams between model *I* and *II* we see that the value of $w_0^{(\text{eff})}$ decreases when the value of α increases, and this means that we can construct more acceptable models for larger values of α . In Fig. 5, the related diagrams of the deceleration parameter $q = q(a; \alpha, K, \mathbf{m}, \mathbf{n}^{(II)})$, for $\mathbf{m} = 0, -1$, $\mathbf{n}^{(II)} = -1$ and $\alpha, K > 0$ are drawn. In the lateral view, the diagrams for the same values of the constant $\mathbf{m}, \mathbf{n}^{(II)}$ for two values $\alpha = 0.01, 0.99$ are pictured. And, in the columnar view, the plots are arranged for the same value of α and different values of $\mathbf{m}, \mathbf{n}^{(II)}$. The present value of the deceleration parameter q_0 is displayed in each plot, which can be calculated as

$$q_0 = -1 + \frac{3}{4} \left[\Omega_0^{(b)}(2 - \mathbf{m}) + \frac{2(1 - K) \left(1 + \Omega_0^{(b)}(\mathbf{m} - 1)\right) \left(1 + \sqrt{27}K^{3/2}\alpha\mathbf{n}^{(II)}\right)}{1 - \sqrt{12}K^{3/2}\mathbf{n}^{(II)}} \right], \quad N = 0, \quad (4.5)$$

which for the special case $\mathbf{n}^{(II)} = 0$ it can be rewritten as

$$q_0 = \frac{3}{4}\Omega_0^{(b)}(1 - 2K)\mathbf{m} + \frac{1}{2} \left(1 - 3K(1 + \Omega_0^{(b)})\right), \quad N = 0, \quad \mathbf{n}^{(II)} = 0. \quad (4.6)$$

It is obvious that the value of q_0 does not depend on α for the models with $\mathbf{n}^{(II)} = 0$, (that is we have $q_0^{(I)} = q_0^{(II)} = q_0^{(III)}$ for $\mathbf{n}'_s = 0$). The related plots are presented in the first row of Fig. 5. As the plots show, for the cases with $\mathbf{n}^{(II)} \neq 0$ an increase in the value of α results in a decrease in the value of q_0 . The models with observationally inconsistent value of q_0 , can be put in an acceptable regime (for which we have $q_0 \simeq -0.6$) by choosing the constant $\mathbf{n}^{(II)}$, properly. This arbitrariness can not be met in GR regime, where $f(R, T) = R$. In GR, observationally consistent values can be achieved only by $K \simeq 1$, irrespective of the value of α , however in $f(R, T)$ gravity one can attain the

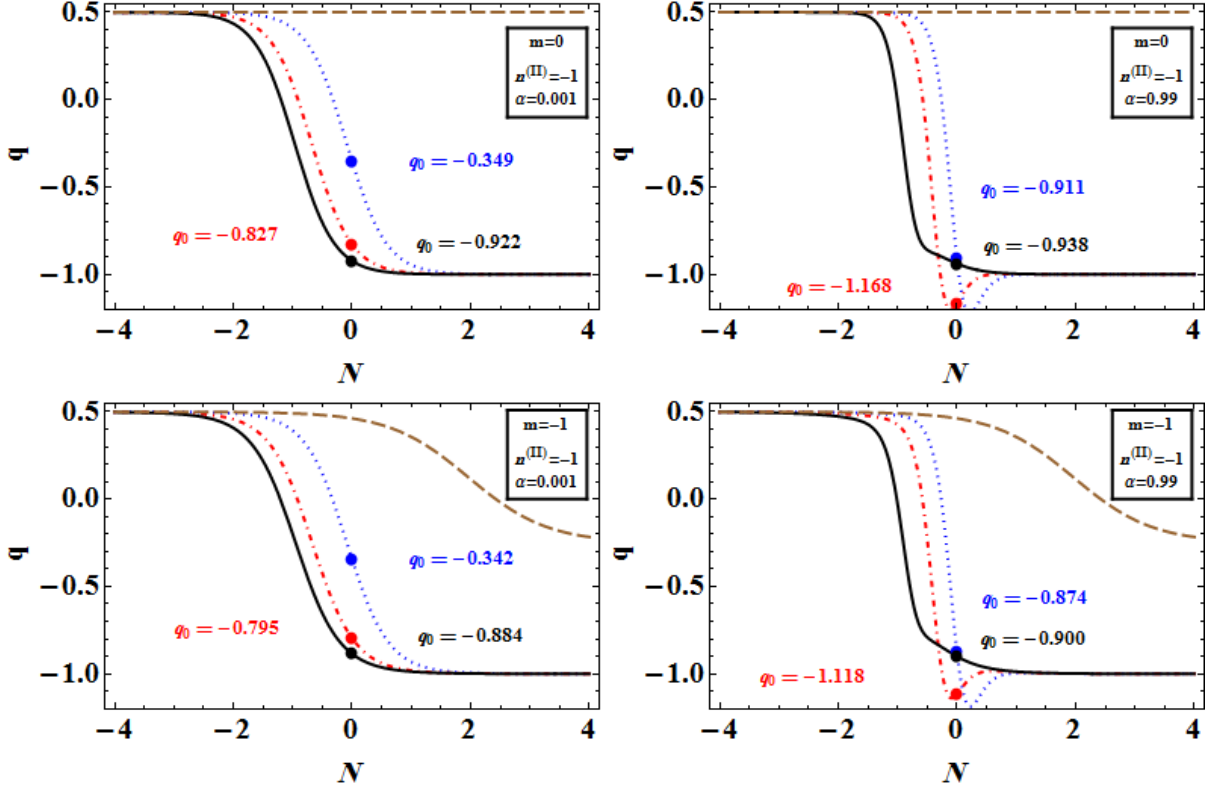


Figure 5. (color online). The evolution of the deceleration parameter for type *II* models for different values of the parameters K , $\mathbf{m} = 0, -1$ and $\mathbf{n}^{(II)} = -1$. The curves are plotted for $K = 0, 0.33, 0.77$ and $K = 0.99$, corresponding to brown dashed line, blue dotted line for, red dotted-dashed line and black solid line. In this case, a lateral view shows that the value of the deceleration parameter decrease when constant α increases. And, a vertical view show that decreasing \mathbf{m} , results in increasing the value of q_0 .

consistent models with arbitrary value K only by a suitable choice of the coupling constant $\mathbf{n}^{(II)}$, (compare the diagrams in the top panels in Fig. 2 with the diagrams in Fig. 5). Comparing the first and the second rows in Fig. 5, shows that turning on the constant \mathbf{m} increases the values of the deceleration parameter. Equation (4.5) show that the present value of the effective EoS (and also the deceleration) parameter for $\mathbf{n}^{(II)} = -1$ are not as simple as result (4.6), and therefore the effect of variation of \mathbf{m} on q_0 is not obvious for each value of K . However, as diagrams in Fig. 5 show, decreasing the value of \mathbf{m} increases the value of q_0 . Comparing the diagrams for model *I* in Fig. 2 with the diagrams in Fig. 5, one can find more acceptable results in model *II* for large values of α .

We have depicted the (r, s) plane diagrams for different values $K = 0.33, 0.77, 0.99$, $\mathbf{m}, \mathbf{n}^{(II)} = 0, -1$ and $\alpha = 0.001, 0.99$ in Fig 6. These diagrams have been arranged in a way that the constant α varies in the horizontal view and the coupling constants $\mathbf{m}, \mathbf{n}^{(II)}$ in the vertical view. Comparison of the lateral diagrams show that, in the high pressure regime an increasing in the value of α decreases the value of s_0 and increases the value of r_0 , so that, this effect is large for the smaller values of K . It means, the distance to the Λ CDM fixed point become so long when α approaches to 1. That is, the models with large values of α and small values of K are distinguishable from the Λ CDM model in the high pressure regime. However, since the Λ CDM is the mostly accepted cosmological model, these models cannot be very interesting. The upper left panel, held for GR regime which resembles the Λ CDM model, since, we have $s_0 \propto -10^{-3}$ and $r_0 \approx 1$. In the vertical view, we see that decreasing the values of \mathbf{m} leads to the distance to Λ CDM fixed point become shorter which is more effective for smaller values of α and K . And, when $\mathbf{n}^{(II)}$ decreases, the present fixed point (s_0, r_0) gets further from Λ CDM one.

C. The model $f^{(III)}(R, T^{(b, c)})$

This case differs the model (*II*) only when $\mathbf{n}^{(III)} \neq 0$. Both models (*II*) and (*III*) have the same behavior for $\mathbf{n}^{(II)} = \mathbf{n}^{(III)} = 0$. The other important point about the model (*III*) is that, the present value of the deceleration parameter q_0 and therefore w_0 , are independent on the values of α for arbitrary values of $\mathbf{n}^{(III)}$. The present value of

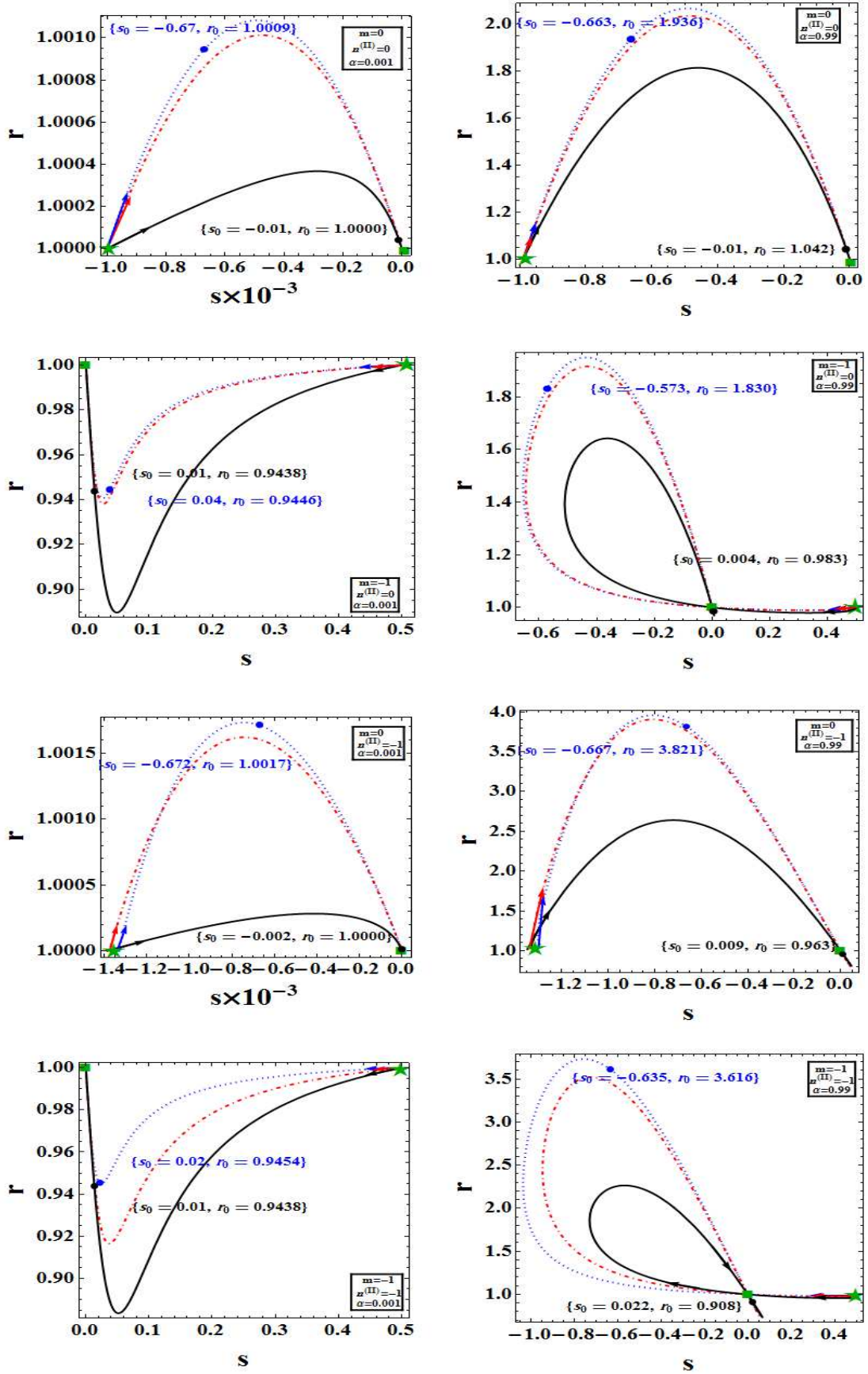


Figure 6. (color online). Cosmological trajectories of model II in the (s, r) plane. The plots show that an increasing in the value of α , has a significant effect on the values of statefinder parameters for smaller values of K , and accordingly, these models have a distinct situation with respect to the the Λ CDM model.

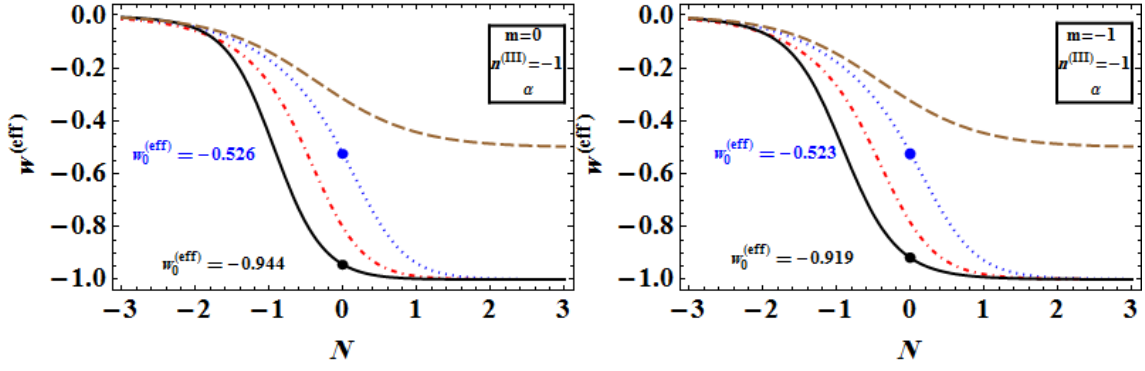


Figure 7. (color online). The evolution of the EoS parameter for model *III*. Here the values of α has no effect on the values of $w^{(\text{eff})}$.

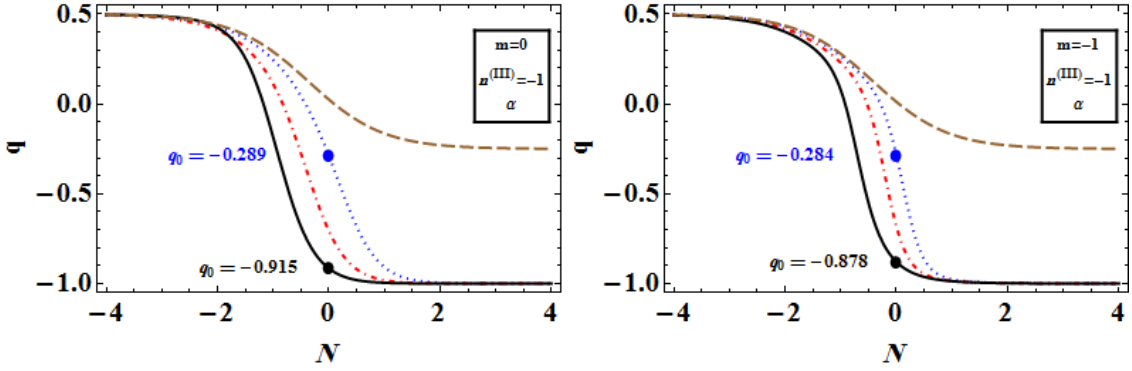


Figure 8. (color online). The evolution of the deceleration parameter for model *III*. The values of q_0 are independent of the values of α .

the deceleration parameter For this model reads

$$q_0^{(\text{III})} = \frac{3}{4(1 - 2\mathbf{n}^{(\text{III})})} \left[\Omega_0^{(\text{b})} \left(1 - 2K(1 - \mathbf{n}^{(\text{III})}) \right) \mathbf{m} - 2 \left(K(\Omega_0^{(\text{b})} - 1) + 2\Omega_0^{(\text{b})} + 1 \right) \mathbf{n}^{(\text{III})} + 2 \left(K(\Omega_0^{(\text{b})} - 1) + 1 \right) \right], \quad N = 0, \quad (4.7)$$

where it indicates that the parameter α does not play any role in the value of $q_0^{(\text{III})}$. In Fig 7 and Fig 8 we present the related diagrams of the effective EoS and the deceleration parameters for $\mathbf{n}^{(\text{III})} = -1$, $\mathbf{m} = 0, -1$, respectively. By indicating the parameter α on diagrams, we emphasis that the present values do not depend on α . The diagrams show that switching the parameter \mathbf{m} on, leads to an increase in the values of w_0 and q_0 . Such an effect appears in model II, as well. Since, when $\mathbf{n}'s = 0$ for three model, we have the same values of w_0 and q_0 , therefore to understand the effect of decreasing the value of $\mathbf{n}^{(\text{III})}$ from zero to an arbitrary negative value (here, -1), one can compare the diagrams of Fig. 8 (or Fig. 7 for the EoS parameter of model III) with the corresponding ones in Fig. 2 (or Fig. 1 for the EoS parameter of model I). we see that, decreasing the values of $\mathbf{n}^{(\text{III})}$, decreases the values of q_0 and w_0 , and the effect is more significant for smaller values of K . Thus, again, decreasing $\mathbf{n}^{(\text{III})}$ to the negative values can help to construct reliable models, with admissible values of w_0 and q_0 . In Figure 9 we present the related diagrams for the statefinder parameters of the model *III*. These diagrams, are plotted for $\mathbf{n}^{(\text{III})} = -1$, since the diagrams for $\mathbf{n}^{(\text{III})} = 0$ are the same as the diagrams for the model *II* with $\mathbf{n}^{(\text{II})} = 0$. As diagrams show, an increasing in the value of α , decreases the value of s_0 and increases the value of r_0 , which this totally leads to the distance to the Λ CDM fixed point become longer. Nevertheless, the effect is weak for larger values of K . And, vertical look say that decreasing \mathbf{m} , have no remarkable effect on the present values of the statefinder parameters, although, leads to the distance become slightly shorter for larger values of α and smaller value of K .

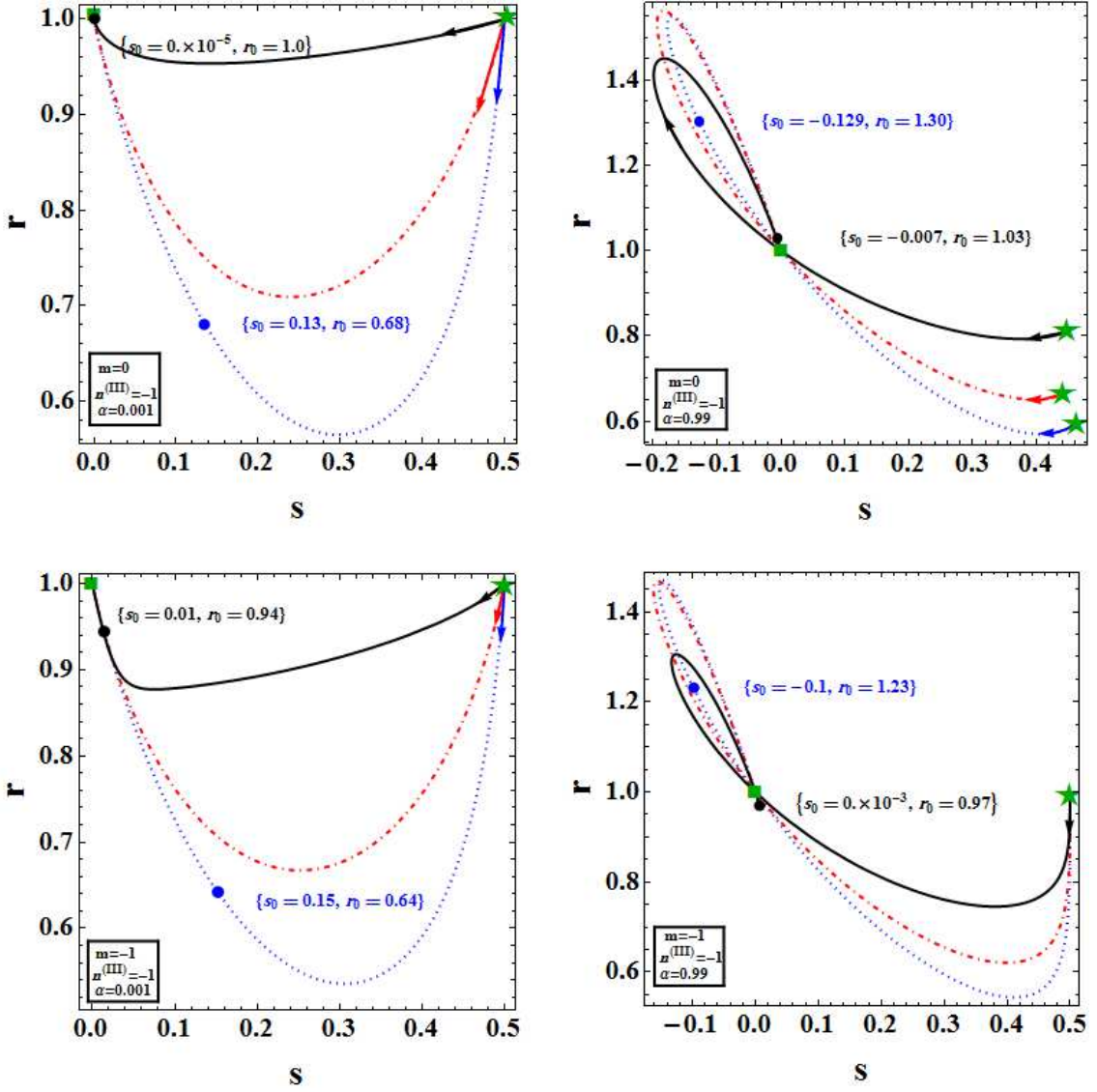


Figure 9. (color online). Statefinder diagnosis of model III in the (s, r) plane. Only the diagrams for $\mathbf{n}^{(III)} = -1$ are plotted since the case $\mathbf{n}^{(III)} = 0$ is as the same as the ones of model II when $\mathbf{n}^{(II)} = 0$. Horizontal view show that if the value of α increases, the distance to the Λ CDM fixed point will slightly enlarge. Also, a decrease in the value of \mathbf{m} has no effective impact on the present values.

V. CONCLUSIONS

In this work we have investigated the cosmological behavior of the generalized Chaplygin gas (GCG) model in $f(R, T)$ theory of gravity endowed by a homogeneous and isotropic FLRW spacetime, by means of statefinder diagnostic. More precisely, the baryonic matter is also included which does not directly interact with the Chaplygin gas. However, these two matters interact with each other via a non standard background geometry. Here, the trace of the whole matter can play the role an secondary factor (besides the metric itself), which relates the evolution of these two type of matters to each other.

In the $f(R, T)$ gravity the conservation of the energy-momentum tensor enforce us to use a constraint equation which must hold by the $f(R, T)$ function. And, this equation gives the form of the $f(R, T)$ function by which the energy-momentum tensor is guaranteed. We solved this equation for two class of models; the models with the standard Chaplygin gas (SCG) and the ones with the GCG gas. All related equations (specially the function $f(R, T)$) of the former are exactly obtained. Nevertheless, the constrained equation can not be exactly solved for the later, because of the appearance of the constant α in the GCG sector. In fact, for each value of this constant (which may be whether integer or not) may there be numerous solution that this involves us a time consuming process of considering these

solutions. To avoid such mathematical problems we approximate the constrain equation in two extreme limits, the high pressure ($p \gg \rho$) and the high density regimes ($\rho \gg p$). Of course, we have supposed that under these two extreme situations, the Chaplygin gas preserves its nature. As a result, we have mainly worked on three models; the models in which SCG is included and we classified them as model I, the GCG models in the high pressure regime, as models II and finally, the GCG models in the high density regime as models III.

After obtaining and then normalizing the Hubble parameter for each model we obtained the deceleration and the statefinder parameters, by which one can differentiate these models, from dark energy (DE) point of view. The statefinder diagnosis is a powerful tools to understand the behavior of different DE scenarios. In our models there are some parameters that capable us to chose the best values for them to make the models consistent with the observations results. The model I contains the constant \mathbf{m} which is related to the coefficient of the baryonic term in the $f(R, T)$ function, $\mathbf{n}^{(I)}$ which corresponds to the SCG term in the $f(R, T)$ function and K which included in the SCG density. In addition to the constants $\mathbf{n}^{(II)}$ and $\mathbf{n}^{(III)}$ which correspond to the GCG term in the $f(R, T)$ function and constant K that comes from GCG density, we have constant α for the other two models. In our work we have used different values for these parameters and plot various diagrams for the effective equation of state (EoS), the deceleration parameter and the statefinder parameters which all are calculated from the modified normalized Hubble parameter for each model. Note that, we have used the present value for the baryonic density parameter which is about five percent of the total matter density parameter. In each diagram we indicate the present values of the related quantities to compare the predictions of the underlying model with the corresponding observational values. Specially, we have plotted the curves of quantities which hold in the GR background (i.e. when the constants \mathbf{m} and \mathbf{n} 's vanish) to compare with the $f(R, T)$ corresponding plots and investigate the possible deviations. We mentioned that the positive values for the constants \mathbf{m} and \mathbf{n} 's lead to some divergencies in diagrams and thus to non-physical results. As a result, we have not followed our considerations for the positive values. The EoS parameter for our models start from the value 0 in the early stage of the evolution of the Universe and converge to -1 , as one expected. Note that, the models of the GCG/SCG in the GR background show a similar behavior [?], (as we also depict this behavior in the diagrams). However, in the $f(R, T)$ gravity the present values improved compared to the corresponding GR ones. As we have shown, in the GR background, only for $K \rightarrow 1$ we have $w_0^{(\text{eff})} \simeq -1$. For example, the values of the EoS parameter for $K = 0.33$ is $w_0^{(\text{eff})(\text{GR})} \simeq -0.314$ which the corresponding values in the three models are; $w_0^{(\text{eff})(I)} \simeq -0.773$ for $\mathbf{m} = 0$ and $\mathbf{n}^{(I)} = -1$, $w_0^{(\text{eff})(II)} \simeq -0.916$ for $\mathbf{m} = -1$, $\mathbf{n}^{(II)} = -1$ and $\alpha = 0.99$, and $w_0^{(\text{eff})(III)} \simeq -0.526$ for $\mathbf{m} = 0$, $\mathbf{n}^{(III)} = -1$ and an arbitrary constant α . Comparing these values we get another important point. For model I and III, the best values are obtained for $\mathbf{m} = 0$, which means when the baryonic term is absent. It shows that in these models the pure SCG/GCG can drive the accelerated expansion of the Universe in the $f(R, T)$ gravity. The better values have obtained in the model II, when a mixture of the baryonic matter and the GCG in the high pressure regime are included. Note that, the larger the constant K becomes, the more observationally accepted values the EoS parameter get. It means that the models *I* and *III* can still be compatible ones provided the the constants K and α be selected properly. However, the model II can give admissible values even for smaller values of K . [for $k=0$ i should explain the special case of cosmological solution in q and w diagram.]

Also, we have investigate these three models in the (s, r) plane, which s and r are the statefinder parameters. This tools can let us to discriminate between different models of DE. In the statefinder diagnosis the difference between the predicted present values s_0 and r_0 of the models and the corresponding values for Λ CDM model (which called the distance to the Λ CDM model) used as a criteria for discrimination of the DE models. Note that, we have $s^{(\Lambda\text{CDM})} = 0$ and $r^{(\Lambda\text{CDM})} = 1$ which this fixed point indicated by a green solid box in our diagrams. We derive these parameters for the three models and plot their evolutionary trajectories for different values of K , \mathbf{m} , \mathbf{n} 's and α . For the clarification purposes, we have also drown the GR corresponding results. In model I, the distance to the Λ CDM model becomes shorter compared to the same model with the GR background. For $\mathbf{m} = -1$ and $\mathbf{n}^{(I)} = 0$ both statefinder parameters slightly closes to the corresponding values for Λ CDM model, and the minimum distance achieved when both \mathbf{m} and $\mathbf{n}^{(I)}$ get the negative values. And, we have shorter distances for the larger values of K , for every values of \mathbf{m} and $\mathbf{n}^{(I)}$. The models of class *I*, can be categorized in two different subclasses based on the initial values of the statefinder parameter s ; some models have trajectories which start from $s = -1/2$, they are corresponding to $\mathbf{m} = 0$, and models with the trajectories which start from $s = +1/2$ with the negative values of \mathbf{m} . In model II, there are several possibilities that can be considered as different scenarios of DE and can be classified in different categories based on their values of the statefinder parameters:

- (i) there are models that are not effectively distinguishable from the Λ CDM model. They have $|s^{(II)} - s^{(\Lambda\text{CDM})}|, |r^{(II)} - r^{(\Lambda\text{CDM})}| \lesssim 10^{-3}$, corresponding to $\alpha \ll 1$.
- (ii) models that have long distance from the Λ CDM model, and they appears when $\mathbf{n}^{(I)} < 0$ and $\alpha \rightarrow 1$.
- (iii) the models that can be accounted for the third class. Their distance are between the one of classes (i) and (ii) and occurs for large values of α . Note that, all cases with $K \rightarrow 1$ have shorter distance than other ones.

In model III all trajectories start from $s = 1/2$ in the (s, r) plane. The distance to the Λ CDM model is nearly independent on the value of α when $\mathbf{n}^{(III)} < 0$. For $\mathbf{n}^{(III)} = 0$, the trajectories are the same as the model II and belong to classes (i) and (iii).

-
- [1] Riess, A.G., *et al.* “Observational evidence from supernovae from an accelerating universe and a cosmological constant”, *Astron. J.* **116** (1998), 1009.
- [2] Perlmutter, S., *et al.* (The Supernova Cosmology Project), “Measurements of Ω and Λ from 42 high-redshift supernovae”, *Astrophys. J.* **517** (1999), 565.
- [3] Riess, A.G., *et al.* “BV RI curves for 22 type Ia supernovae”, *Astron. J.* **117** (1999), 707.
- [4] Spergel, D, N, *et al.* “First year wilkinson microwave anisotropy probe (WMAP) observations: determination of cosmological parameters”, *Astrophys. J. Suppl.* **148** (2003) ,175.
- [5] Spergel, D, N, *et al.* “Wilkinson microwave anisotropy probe (WMAP) three year results: implications for cosmology”, *Astrophys. J. Suppl.* **170** (2007) ,377.
- [6] Komatsu, E, *et al.* “Five-Year wilkinson microwave anisotropy probe (WMAP) observations: cosmological interpretation”, *Astrophys. J. Suppl.* **180** (2009) ,330.
- [7] Komatsu, E, *et al.* “Seven-Year wilkinson microwave anisotropy probe (WMAP) observations: cosmological interpretation”, *Astrophys. J. Suppl.* **192** (2011) ,18.
- [8] Hinshaw, G.F., *et al.* “Nine-Year wilkinson microwave anisotropy probe (WMAP) observations: cosmological parameter results”, *Astrophys. J. Suppl.* **208** (2013) ,19.
- [9] Bertonea, G., Hooperb, D. & Silk, J. “Particle dark matter: evidence, candidates and constraints”, *Phys. Rep.* **405** (2005), 279.
- [10] Silk, J. “Dark matter and galaxy formation”, *Ann. Phys. (Berlin)* **15** (2006), 75.
- [11] Feng, J.L. “Dark matter candidates from particle physics and methods of detection”, *Annu. Rev. Astron. Astrophys.* **48** (2010), 495.
- [12] Bergström, L. “Dark matter evidence, particle physics candidates and detection methods”, *Ann. Phys. (Berlin)* **524** (2012), 479.
- [13] Frenk, C.S. & White, S.D.M. “Dark matter and cosmic structure”, *Ann. Phys. (Berlin)* **524** (2012), 507.
- [14] Peebles, P.J.E. “The cosmological constant and dark energy”, *Rev. Mod. Phys.* **75** (2003), 559.
- [15] Polarski, D. “Dark energy: current issues”, *Ann. Phys. (Berlin)* **15** (2006), 342.
- [16] Copeland, E.J., Sami, M. & Tsujikawa, S. “Dynamics of dark energy”, *Int. J. Mod. Phys. D* **15** (2006), 1753.
- [17] Durrer, R. & Maartens, R. “Dark energy and dark gravity: theory overview”, *Gen. Rel. Grav.* **40** (2008), 301.
- [18] Ade, P.A.R., *et al.* “Planck 2013 results. XVI. cosmological parameters”, *A&A* **571** (2013), A16.
- [19] Ade, P.A.R., *et al.* “Planck 2015 results. XIII. cosmological parameters”, *astro-ph/1502.01589*.
- [20] Ostriker, J.P. & Steinhardt, P.J. “Cosmic concordance”, *astro-ph/9505066*.
- [21] Weinberg, S. “The cosmological constant problem”, *Rev. Mod. Phys.* **61** (1989), 1.
- [22] Nobbenhuis, S. “The cosmological constant problem, an inspiration for new physics”, *gr-qc/0609011*.
- [23] Padmanabhan, H. & Padmanabhan, T. “CosMIn: The solution to the cosmological constant problem”, *Int. J. Mod. Phys. D* **22** (2013), 1342001.
- [24] Bernard, D. & LeClair, A. “Scrutinizing the cosmological constant problem and a possible resolution”, *Phys. Rev. D* **87** (2013), 063010.
- [25] Chiba, T., Okabe, T. & Yamaguchi, M. “Kinetically driven quintessence”, *Phys. Rev. D* **62** (2000), 023511.
- [26] Armendariz-Picon, C., Mukhanov, V. & Steinhardt, P.J. “Dynamical solution to the problem of a small cosmological constant and late-time cosmic acceleration”, *Phys. Rev. Lett.* **85** (2000), 4438.
- [27] Sheykhi, A. & Bagheri, A. “Quintessence ghost dark energy model”, *Europhys. Lett.* **95** (2011) , 39001.
- [28] Saridakis, E., N. & Ward, J. “Quintessence and phantom dark energy from ghost D-branes”, *Phys. Rev. D* **80** (2009), 083003.
- [29] Kamenshchik, A., Moschella, U., & Pasquier, V., “An alternative to quintessence”, *Phys. Lett. B* **511** (2001) , 265.
- [30] Fabris, J., C., Gonalves, S., V., B., & de Souza, P., E. “Density perturbations in a universe dominated by the Chaplygin gas”, *Gen. Rel. Grav.* **34** (2002), 53.
- [31] Bento, M., C., Bertolami, O., & Sen, A., A. “Generalized Chaplygin gas, accelerated expansion and dark energy-matter unification”, *Phys. Rev. D* **66** (2002), 043507.
- [32] Avelino, P., P., *et al.* “Alternatives to quintessence model building”, *Phys. Rev. D* **67** (2003), 023511.
- [33] Bean, R., & Dore, O. “Are Chaplygin gases serious contenders for the dark energy?”, *Phys. Rev. D* **68** (2003), 023515.
- [34] Sandvik, S., B., Tegmark, M., Zaldarriaga, M., & Waga, I. “The end of unified dark matter?” *Phys. Rev. D* **69** (2004), 123524.
- [35] Ebadi, H., & Moradpour, H. “Thermodynamical description of modified generalized Chaplygin gas model of dark energy”, *Int. J. Theor. Phys.* **55** (2016), 1612.
- [36] Dindam, B., R., Kumar, S., & Sen, A., A. “Inflationary generalized Chaplygin gas and dark energy in the light of the Planck and BICEP2 experiments”, *Phys. Rev. D* **90** (2014), 083515.
- [37] Fabris, J., C., Goncalves, S., V., B., Velten, H., E., S., & Zimdahl, W. “Matter Power Spectrum for the Generalized

- Chaplygin Gas Model: The Newtonian Approach”, *Phys. Rev. D* **78** (2008), 103523.
- [38] Eiroa, E., F. “Thin-shell wormholes with a generalized Chaplygin gas”, *Phys. Rev. D* **80** (2009), 044033.
- [39] Bejarano, C., & Eiroa, E., F. “Dilaton thin-shell wormholes supported by a generalized Chaplygin gas”, *Phys. Rev. D* **84** (2011), 064043.
- [40] Farhoudi, M. “On higher order gravities, their analogy to GR, and dimensional dependent version of Duff’s trace anomaly relation”, *Gen. Rel. Grav.* **38** (2006), 1261.
- [41] Nojiri, S. & Odintsov, S.D. “Introduction to modified gravity and gravitational alternative for dark energy”, *Int. J. Geom. Meth. Mod. Phys.* **04** (2007), 115.
- [42] De Felice, A. & Tsujikawa, S. “ $f(R)$ theories”, *Living Rev. Rel.* **13** (2010), 3.
- [43] Sotiriou, T.P. & Faraoni, V. “ $f(R)$ theories of gravity”, *Rev. Mod. Phys.* **82** (2010), 451.
- [44] Ziaie, A., H., Atazadeh, K., & Rasouli, S. M. M. “Naked Singularity Formation In $f(R)$ Gravity”, *Gen. Rel. Grav.* **43** (2011), 2943.
- [45] Bertolami, O., Böhmer, C.G., Harko, T. & Lobo, F.S.N. “Extra force in $f(R)$ modified theories of gravity”, *Phys. Rev. D* **75** (2007), 104016.
- [46] Bertolami, O. & Páramos, J. “Do $f(R)$ theories matter”, *Phys. Rev. D* **77** (2008), 084018.
- [47] Bertolami, O., Lobo, F.S.N., & Páramos, J. “Nonminimal coupling of perfect fluids to curvature”, *Phys. Rev. D* **78** (2008), 064036.
- [48] Harko, T. “Modified gravity with arbitrary coupling between matter and geometry”, *Phys. Lett. B* **669** (2008), 376.
- [49] Nesseris, S. “Matter density perturbations in modified gravity models with arbitrary coupling between matter and geometry”, *Phys. Rev. D* **79** (2009), 044015.
- [50] Harko, T. & Lobo, F.S.N. “ $f(R, L_m)$ gravity”, *Eur. Phys. J. C* **70** (2010), 373.
- [51] Harko, T., Lobo, F.S.N., Nojiri, S. & Odintsov, S.D. “ $f(R, T)$ gravity”, *Phys. Rev. D* **84** (2011), 024020.
- [52] Houndjo, M.J.S., Alvarenga, F.G., Rodrigues, M.E., Jardim, D.F. & Myrzakulov, R. “Thermodynamics in little rip cosmology in the framework of a type of $f(R, T)$ gravity”, *gr-qc/1207.1646*.
- [53] Sharif, M. & Zubair, M. “Thermodynamics in $f(R, T)$ theory of gravity”, *J. Cosmol. Astropart. Phys.* **03** (2012), 028.
- [54] Jamil, M., Momeni, D. & Ratbay, M. “Violation of the first law of thermodynamics in $f(R, T)$ gravity”, *Chin. Phys. Lett.* **29** (2012), 109801.
- [55] Sharif, M. & Zubair, M. “Thermodynamic behavior of particular $f(R, T)$ -gravity models”, *J. Exp. Theor. Phys.* **117** (2013), 248.
- [56] Alvarenga, F.G., Houndjo, M.J.S., Monwanou, A.V. & Chabi Orou, J.B. “Testing some $f(R, T)$ gravity models from energy conditions”, *J. Mod. Phys.* **04** (2013), 130.
- [57] Shabani, H., & Farhoudi, M. “ $f(R, T)$ cosmological models in phase-space”, *Phys. Rev. D* **88** (2013), 044048.
- [58] Shabani, H., & Farhoudi, M. “cosmological and solar system consequences of $f(R, T)$ gravity models”, *Phys. Rev. D* **88** (2014), 044031.
- [59] Sahni, V., Saini, T., D., Starobinsky, A., A., & Alam, U. “Statefinders a new geometrical diagnostic of dark energy”, *JETP Lett.* **77** (2003), 201.
- [60] Alam, U., Sahni, V., Saini, T.D. & Starobinsky, A.A. “Exploring the expanding Universe and dark energy using the statefinder diagnostic”, *Mon. Not. R. Astron. Soc.* **344**, (2003), 1057.
- [61] Zimdahl, W. & Pavon, D. “Letter: statefinder parameters for interacting dark energy”, *Gen. Rel. Grav.* **36** (2004), 1483.
- [62] Zhang, X. “Dark energy constraints from the cosmic age and supernova”, *Phys. Lett. B*, **611** (2005), 1.
- [63] Zhang, X. “Statefinder diagnostic for holographic dark energy model”, *Int. J. Mod. Phys. D*, **14** (2005), 1597.
- [64] Zhang, J., Zhang, X. & Liu, H. “Statefinder diagnosis for the interacting model of holographic dark energy”, *Phys. Lett. B*, **659** (2008), 26.
- [65] Setare, M.R., Zhang, J. & Zhang, X. “Statefinder diagnosis in a non-flat universe and the holographic model of dark energy”, *J. Cosmol. Astropart. Phys.*, **0703** (2007), 007.
- [66] Chang, B.R., Liu, H.Y., Xu, L.X., Zhang, C.W. & Ping, Y.L. “Statefinder parameters for interacting phantom energy with dark matter”, *J. Cosmol. Astropart. Phys.*, **0701** (2007), 016.
- [67] Shao, Y. & Gui, Y. “Statefinder parameters for tachyon dark energy model”, *Mod. Phys. Lett. A*, **23** (2008), 65.
- [68] Malekjani, M., Khodam-Mohammadi, A. & N. Nazari-Pooya, “Generalized Chaplygin gas model: cosmological consequences and statefinder diagnosis”, *Astrophys. Space Sci.*, **334** (2011), 193.
- [69] Zhang, L., Cui, J., Zhang, J., Zhang, X. “Interacting model of new agegraphic dark energy: cosmological evolution and statefinder diagnostic”, *Int. J. Mod. Phys. D*, **19** (2010), 21.
- [70] Khodam-Mohammadi, A. & Malekjani, M. “Cosmic behavior, statefinder diagnostic and $w - w'$ analysis for interacting new agegraphic dark energy model in non-flat universe”, *Astrophys. Space Sci.*, **331** (2010), 265.
- [71] Capozziello, S. & Faraoni, V., *Beyond Einstein Gravity*, (Springer, Netherlands, 2011).